Organic Draw Solutions and their Temperature Effects for Renewable Electricity Production by Closed-Loop Pressure Retarded Osmosis

Suman Adhikary

A Thesis

In

The Department

of

Building, Civil & Environmental Engineering

Presented in Partial Fulfillment of the Requirements
For the Degree of
Master of Applied Science (Civil Engineering) at
Concordia University
Montreal, Quebec, Canada.

March 2019

CONCORDIA UNIVERSITY

School of Graduate Studies

This is to certify that the thesis prepared

By: Suman Adhikary

Entitled: Organic Draw Solutions and their Temperature Effects for Renewable Electricity Production by Closed-Loop Pressure Retarded Osmosis

and submitted in partial fulfillment of the requirements for the degree of

Master of Applied Science (Civil Engineering)

complies with the regulations of the University and meets the accepted standards with respect to originality and quality. Signed by the final Examining Committee:

_____ Chair
Dr. S. Samuel Li

_____ Examiner
Dr. Mamoun Medraj

_____ Examiner
Dr. Catherine Mulligan

_____ Co-Supervisor
Dr. Saifur Rahaman

_____ Co-Supervisor
Dr. Amruthur S. Ramamurthy

Approved by,

_____ Graduate Program Director
Dr. Fariborz Haghighat

_____ Dean of Faculty
Dr. Amir Asif

Date: _____ 2019

Abstract

Organic Draw Solutions and their Temperature Effects for Renewable Electricity Production by Closed-Loop Pressure Retarded Osmosis

The urge to use sustainable green energy to meet the ever-increasing energy demand is inevitable due to the depletion of existing fossil fuels sources. Closed-loop pressure retarded osmosis (PRO) process is one of the renewable technologies which can produce green energy without having any deleterious effects on nature. It is a process which combines both PRO (source of generating power) and a downstream separation process, such as membrane distillation (MD), for the regeneration of draw solution. An appropriate draw solution selection is a key to successful implementation of closed-loop PRO process for sustainable energy generation. In this study, few organic compounds such as potassium citrate (KCit), calcium acetate (CaAc), potassium oxalate (KOxa), potassium acetate (KAc), ammonium acetate (NH_4Ac), ammonium carbamate (NH_4C), ammonium formate (NH_4F), potassium formate (KF), sodium glycolate (NaGly), sodium propionate (NaP) and calcium propionate (CaP) were identified for the first time as highly effective draw solutions (except for NaP). Using a desktop screening method, the organic compounds were identified by considering physical state at ambient condition, water solubility, and osmotic pressure. The draw solutions were comprehensively evaluated for water flux, power density and reverse salt flux through a laboratory-based investigation of the PRO process. The peak power densities achieved for the identified draw solutions were 5.32 W/m^2 to 6.73 W/m^2 at a 2.8 MPa osmotic pressure. These peak power densities increased from 109% to 118% (11.1 W/m^2 to 14.64 W/m^2) when increasing the osmotic pressure of the draw solutions by 50% (i.e. 4.2 MPa). A significant increase in the peak power density was obtained due to the very low reverse salt flux for the organic draw solutions (0.029 to 0.0699 mol m^{-2} h^{-1} and 0.0325 to 0.0854 mol m^{-2} h^{-1} at osmotic pressures of 2.8 MPa and 4.2 MPa, respectively). The identified organic draw solutions were also analyzed as distillable and thermolytic through gravimetric method for the identification of potential downstream recovery methods to recycle the draw solutions in the closed-loop PRO process. This research concludes that, except for ammonium carbamate, all other

aforementioned draw solutions could be potentially recovered using the membrane distillation process.

As the temperature is directly associated with solution physicochemical properties, this research has been further extended to observe the effect of temperature on the performance enhancement of the closed-loop PRO process. The effect of temperature has been studied on two organic draw solutions, potassium acetate (KAc) and sodium propionate (NaP), due to a similar osmotic pressure with NaCl. It has been found that KAc and NaP show ~31% (8.5 Wm^{-2} to 11.1 Wm^{-2}) and ~27% (8.1 Wm^{-2} to 10.3 Wm^{-2}) increase respectively in power density while increasing the operating temperature from 20^0C to 40^0C. It has been further investigated that reversal salt flux is ~5-8 times lower for organic salt than NaCl. A comparison shows that at 40^0C, potassium acetate and sodium propionate produce 23% and 14.5% higher power density over sodium chloride draw solution. Based on the result of this study, increased power production coupled with a lower reversal salt flux has made organic salt as a potential draw solution for the future research in the PRO process.

Acknowledgments

I would like to express my profound thankfulness and sincere gratitude to my Co-supervisor, Dr. Saifur Rahaman, for his constant guidance and inspirations throughout the study. His extreme helpfulness as well as vast knowledge, expertise and patience during correcting my writing is always very much encouraging. I am also indebted to my supervisor for providing me the opportunity to work with such an incredible and ever helpful research group.

I would also like to acknowledge my sincere gratitude to my co-supervisor Dr. Amruthur S Ramamurthy, for his valuable insights and support throughout this research work.

I also would like to extend my special thanks to the lab technicians for preparing the lab experimental setup.

Table of Contents

List of Figures

List of Tables

List of Abbreviations

PRO	Pressure Retarded Osmosis
MD	Membrane Distillation
KCit	Potassium Citrate
CaAc	Calcium Acetate
KOxa	Potassium Oxalate
KF	Potassium Formate
NH_4Ac	Ammonium Acetate
NH_4C	Ammonium Carbamate
NH_4F	Ammonium Formate
NaGly	Sodium Glycolate
NaP	Sodium Propionate
CaP	Calcium Propionate
KAc	Potassium Acetate
NaCl	Sodium Chloride
NH_4HCO_3	Ammonium Bicarbonate
MPa	Mega Pascal
TFC	Thin-Film Composite
FO	Forward Osmosis
LMH	Liter/m^2-hr
R	Rejection
R_1	Universal Gas Constant
π	Osmotic Pressure
ρ	Density
μ	Kinematic Viscosity
υ	Dynamic Viscosity
T	Temperature in Kelvin Unit

m	Molality
A	Water Permeability Co-efficient
B	Salt Permeability Co-efficient
CP	Concentration Polarization
ICP	Internal Concentration Polarization
ECP	External Concentration Polarization
DI	De-ionized
CA	Cellulose Acetate
HTI	Hydration Technology Innovations
FRQNT	Fonds de recherche du Québec-Nature et technologies

Chapter 1: Introduction

1.1 Rationale

Dependence on fossil fuel is unsustainable and heavy reliance on fossil fuel like coal, oil and natural gas is accelerating changes toward deteriorating long-term effects on the environment. There is a growing need to look for renewable energy sources to meet the ever-increasing energy demand. Pressure retarded osmosis (PRO) is an osmotically driven membrane-based process which harnesses the osmotic pressure differences between two solutions of different salinity gradients and produces energy in the form of electricity without producing CO_2 [1]. It is an emerging green technology as it does not produce any greenhouse gasses (GHGs). Open-loop and closed-loop PRO are the two types of PRO process. The diluted draw solution is discharged in the open-loop PRO process, whereas the draw solution with osmotic potential is regenerated instead of discharged during the closed-loop PRO process. Closed-loop PRO is more advantageous than open loop PRO in terms of performance, efficiency and environmental consideration. The ability to utilize low-grade waste heat in closed-loop PRO is another very crucial aspect for the sustainability of the total system. Installment of closed-loop PRO system within the close proximity of power plants, solar panels or breweries where a large amount of energy is being lost as waste heat process can make this process even more feasible. In closed-loop PRO, selection of the draw solution plays a very important role for the overall performance of this process. Keeping this aspect in mind, extensive desktop screening analysis has been conducted to find suitable draw solutions for the closed-loop PRO process.

Another interesting feature for closed-loop PRO is the operating temperature effect. Since temperature is directly associated with solution physicochemical properties, increasing of operating temperature can be influential for the performance enhancement of the PRO process [2-3]. This study has therefore been further extended to observe how temperature can affect the overall efficiency of this process.

1.2 PRO – An Emerging Technology

PRO is a process which utilizes the chemical potential of two solutions with different salinity gradients. In this osmotically driven process, low salinity and high salinity solutions are being separated by a semi-permeable membrane. In the natural osmosis process, fresh water moves from low concentration to high concentration solutions. Similarly, in the PRO process, fresh water from the low saline solution passes through the semipermeable membrane towards the high saline solution. Except for all the similarity with the natural osmosis process, the high saline solution (also called the draw solution) is pressurized in PRO process. Due to the volumetric expansion of the pressurized draw solution, hydraulic pressure develops in the draw solution side. This pressurized draw solution eventually runs a turbine, converting hydraulic pressure into electrical energy. In essence, PRO utilizes the osmotic potential difference between two sides of the membrane using two different solutions with different salinity gradients and convert the chemical potential difference into power. There are many advantages of the PRO process over other renewable sources which are as follows:

- Sustainable and environmentally friendly technology since there are no GHG emissions (no CO_2 emissions);
- Utilizes the energy between two different salinity gradient solutions;
- Can utilize the low-grade waste heat by converting into electrical energy; and
- Unlike solar and wind turbines, PRO is a continuous process and supply energy without interruption.

1.3 Classifications of PRO

PRO can be classified into two categories; – open-loop PRO process (also can be termed as natural PRO) and closed-loop PRO process. The open-loop PRO process deals with seawater, river water and the brine from the reverse osmosis processes. The draw solution used in this process is NaCl. There are a few limitations of this process such as:

- For running the open-loop PRO, it needs to be near the bay area where river water and seawater mixes;

- The management of draw solution is a problem since the draw solution has to be discharged eventually; and
- The existing membrane for PRO is very much prone to reversal salt flux for salt like NaCl.

However, closed-loop PRO processes can outperform open-loop PRO for many reasons. There is no limitation for utilizing the draw solution. Different draw solutions with superior applicability can be selected. Also, the reversal salt flux phenomenon can be properly addressed when running closed-loop PRO. Most importantly, the diluted draw solution can be regenerated and utilized in the process repeatedly. To conclude, the closed-loop PRO process has attractive features in terms of overall performance, in terms of efficiency, in terms of regeneration of draw solution and in terms of the being an environmental friendly system. Moreover, the operation of the closed-loop PRO process is not limited to any specific location (for example bay area).

1.3.1 Features of closed-loop PRO

Closed-loop PRO comprises of three main parts, namely the PRO unit for the utilization of osmotic pressure difference between two different salinity gradient solutions, the water turbine for generation of power and the downstream separation process for the regeneration of draw solution. Due to several additional advantages of closed-loop PRO over open-loop PRO, it's gaining popularity.

1.4 Selection of draw solution

Performance of the PRO processes, such as the water flux or reversal salt flux, largely depends on the properties of the draw solution. This shows the importance of choosing an appropriate draw solution. Some crucial parameters should be taken into consideration before choosing draw solutions such as the physical state of draw solute at ambient temperature and pressure, toxicity, solubility and osmotic pressure of the draw solution [2]. Using these parameters, comprehensive desktop screening processes may identify potential draw solutions.

1.5 Temperature effect on closed-loop PRO performance

Raising the temperature of the PRO process is associated with changing the properties such as viscosity, density, diffusivity and the osmotic pressure of the draw solution [3]. These property changes emphasize the reasoning of studying the temperature effects on different draw solutions, and how this changes the overall performance of the whole PRO process.

1.6 Objectives of the study

The objectives of this study are as follows:

- To find appropriate draw solutions for closed-loop PRO process for the successful implementation of the process;
- To evaluate performance enhancement for different draw solutions and analyze the performance of the whole system;
- To make a comparative study on identified draw solutions with the most commonly used NaCl and $NaHCO_3$;
- To observe the increased temperature effect by utilizing waste heat and to study the performance enhancement of the closed-loop PRO for selected draw solutions;
- To verify the experimental result of the temperature effect for the selected draw solution with numerical analysis; and
- To perform a sensitivity analysis on the temperature effect for the selected draw solution over most commonly used NaCl draw solution.

1.7 Organization of the dissertation

The dissertation comprises following sections:

Section 1: A short introduction which describes the motivation of the study, a general overview of the overall process and objectives of the study;

Section 2: A brief description of the reviewed literature of PRO process, state of the art technology for PRO, research gap, a summary of draw solutions used for PRO;

Section 3: Highly effective organic draw solutions for renewable power generation by closed-loop pressure retarded osmosis;

Section 4: Effect of temperature on closed-loop PRO with potential organic draw solution; and

Section 5: This section covers the conclusion and recommendations for future directions.

Chapter 2: Literature review

2.1 Background

Dependence on fossil fuel is unsustainable and heavy reliance on fossil fuel like coal, oil and natural gas is accelerating changes toward deteriorating long-term effects. There is a need for renewable energy sources to meet the ever-increasing energy demand. Studies demonstrate that renewable energies can power the world with an energy potential of 10,000 TWh every year [1]. As we can see from Figure 1, 11% of the total energy consumption is coming from renewable sources. The sources include biofuels, solar, wind, geothermal and hydroelectricity. Among all the renewable energy sources, hydro-electric sources have an enormous potential to produce energy [59].

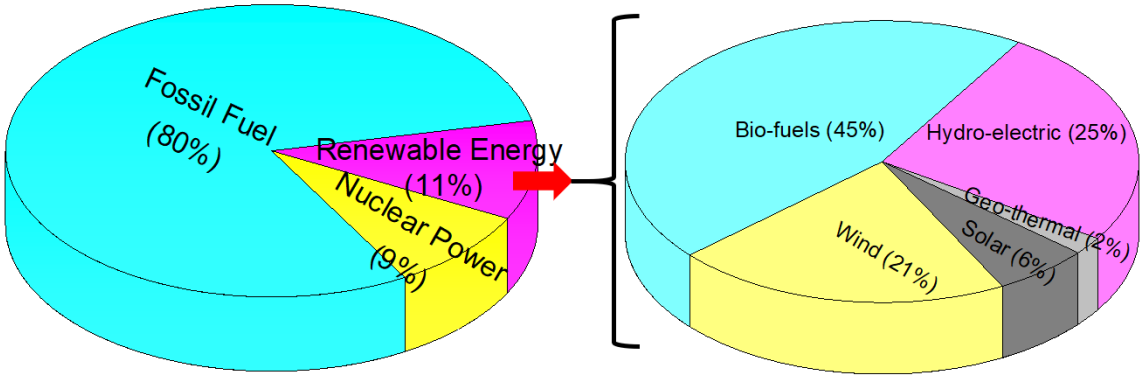

Figure 1 Energy consumption based on energy sources

A type of renewable and gas emission-free energy that has just recently been given credibility is salinity-gradient energy, which is based on the release of free energy upon mixing of waters with different salt concentration solutions. [4]. In the world of hydroelectric generation systems, the use of salinity gradient energy has the highest energy concentration and can produce approximately 1650 TWh every year, making it a viable source of electricity [6-7].

Desalination requires ΔG_{sep} (= Gibbs free energy) to get clean water and salt. The opposite, or by mixing salt and water, we can harness back the ΔG_{mix} (i.e. opposite of ΔG_{sep}). By utilizing this concept, further explained in Figure 2, power in the form of electricity can be generated.

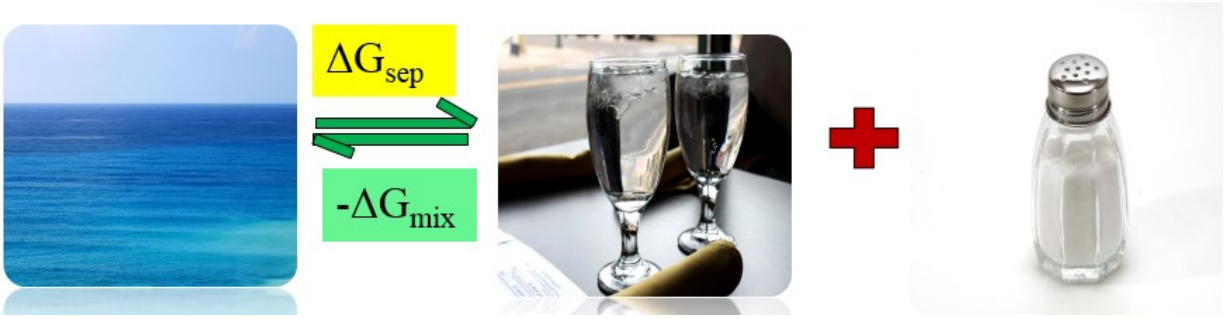

Figure 2 Concept of harnessing energy by mixing two different salinity gradient solution

2.2 Overview of PRO

PRO process is used to generate electricity when two solutions with different salinity gradient are mixed. In this membrane-based osmotic process, pressure energy due to hydraulic pressure is recovered when water is transported from the diluted to the concentrated solution through a semi-permeable membrane. Due to the difference between the osmotic pressure of the two side of the membrane, water will pass through the membrane from the low to high salinity solution. The volumetric expansion of this high saline solution releases into the turbine to generate electricity [7].

In the PRO process, fresh water, wastewater, and very low saline water are normally used as feed solution while high concentration solution like seawater, RO brine concentrates, and high concentration salt solutions (laboratory mixed salts) is used as draw solution. Usually, the draw solution is chosen in such a way that it can be separated conveniently when applying downstream separation processes, such as membrane distillation (MD) or thermal distillation separation.

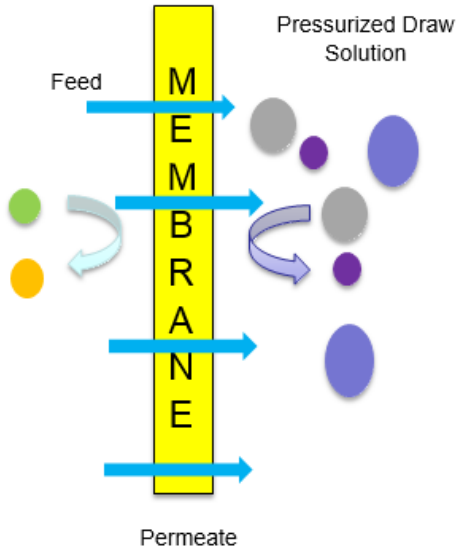

Figure 3 Mechanism of PRO process

2.3 Historical development of PRO

2.3.1 Early studies (1950s)

The idea of utilizing energy from two different salinity gradient solutions were first developed during the early 1950s [5]. Many researchers have modified the technique and improved over time. PRO has improved a lot and gained popularity since then. One of the most important features of the PRO process is that it can produce electricity without any disruption and without the production of greenhouse gases (GHGs). In 1954, Pattle first reported that the energy can be harnessed by the mixing of salt and fresh water [4]. Pattle demonstrated that when freshwater with a volume "V" mixes with the much larger volume of salty water of osmotic pressure "π", the free energy lost is equivalent to "πV". Pattle also illustrated that when seawater and river water mixes, it dissipates the energy equal to that obtainable from a waterfall of 680 ft high [4]. However, no paper was published for the next 20 years to observe any experimental analysis until Norman designed a system that was able to produce energy by running a water wheel by effectively utilizing the concept by converting chemical potential into hydrostatic potential [8].

2.3.2 The 1970s

The oil crisis in 1973 revived the search for finding renewable sources. The concept proposed by Pattle was further analyzed be several papers [9–15]. Norman [8] was able to demonstrate that freshwater could permeate through a selectively permeable membrane into a pressurized seawater chamber, and then the spillover water could turn a water wheel to power a generator. In 1975, Loeb and Norman [14] proposed PRO based on the osmotic-driven membrane process. After one year another paper using a standard RO membrane was published [9], where hollow fiber seawater RO membranes were tested using freshwater in the bore and pressurized brine in the shell. Further experimental investigations have been completed by Loeb and Mehta [11–13], successfully justifying the PRO concept and revealing power outputs (from 1.56 to 3.27 Wm^{-2} using hypersaline draw solutions). However, the practical power output is very small due to the poor membrane (from 1.56 to 3.27 Wm^{-2} using hypersaline draw solutions) performance.

2.3.3 The 1980s

In 1980s, four papers were published where more theoretical and experimental analysis was completed to check the feasibility of the PRO process [16–19]. The authors believed that discovered power densities could justify the construction of a cost-competitive osmotic power plant. Lee et al. [15] developed a model considering the effect of the internal concentration polarization (ICP) while neglecting the external concentration polarization (ECP), to evaluate the power density and water flux. However, the model proposed by Lee et al. [15] served as a reference model for future investigation. The general equation Lee et al. [15] used to describe water transport in PRO was:

$$J_w = A\,(\Delta\pi_m - \Delta P) \quad \text{.....(1)}$$

Where A is water the permeability coefficient, $\Delta\pi_m$ is the effective osmotic pressure difference between draw and feed solution and ΔP is the applied hydraulic pressure.

Power density obtained from the PRO process is the product of water flux and applied pressure which is as follows:

$$W = J_w * \Delta P \quad \text{..... (2)}$$

Fig.4 explains the zones of different osmosis processes as a function of applied pressure. The theoretical operational limit of PRO is defined at the point where applied pressure equals the osmotic pressure difference.

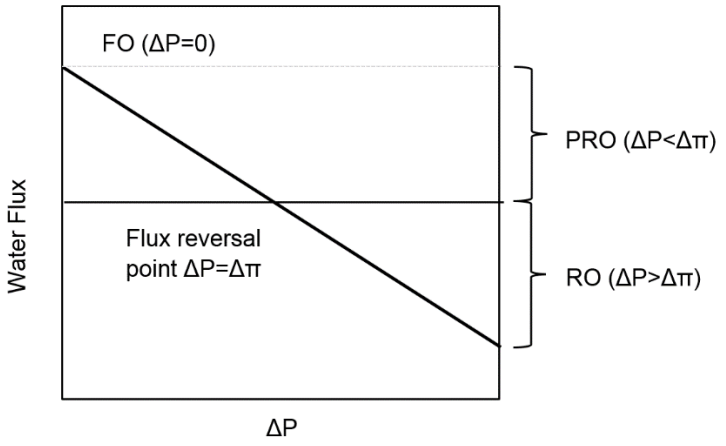

Figure 4 PRO zone (ΔP<Δπ), RO zone (ΔP>Δπ), FO zone (ΔP=0) and flux reversal point PRO (ΔP=Δπ), shown as a function of applied pressure.

2.3.4 The 1990s

In 1990, Loeb et al. [19] studied mechanical efficiencies for several plant configurations utilizing a pressure-retarded osmosis (PRO) energy converter. The authors investigated three different PRO configurations, namely the continuous-flow terrestrial PRO facility, a continuous-flow underground PRO facility, and an alternating-flow terrestrial PRO facility in order to find the mechanical efficiencies. It was found that the alternating-flow terrestrial PRO plant had a higher efficiency but required the use of two pressure vessels in addition to the usual PRO equipment. Reali et al. [20] were able to predict the salt concentration profiles developing in the porous support layer of the anisotropic membrane. These concentration profiles were evaluated by means of an analytical-numerical technique applied to specific boundary-value problems based on the steady-state convective-diffusion equation for the salt concentration. This study highlighted the role of key membrane characteristics such as water permeability coefficient (A), salt permeation coefficient (B), the thickness of the porous support layer (t), and effective salt diffusivity (D) on the water and salt permeation through the membrane [20].

Loeb et al. [21] investigated the economics of PRO to observe whether the cost of energy production is compatible with the United States retail electricity price. He suggested that depending on system configurations, electrical energy could be produced at a cost ranging from 0.058 to 0.07 $/kWh — costs comparable to the average retail electricity price in the United States at that time (0.067 $/kWh) [22].

2.3.5 The 2000s

In 2000, Loeb started investigating with Great Salt lake and found the possibilities of osmotic power potential which is around 0.15 $/kWh [23]. After two years, Loeb [24] developed the first successfully incorporated Pressure Exchanger (PX), enabling Loeb to demonstrate cost-effective PRO systems. Loeb thus published a paper that described an improved plant schematic incorporating the PX. In 2004, Seppälä suggested [25] that the apparent nonlinearity of the osmotic pressure is caused by concentration polarization phenomena. After that, Norwegian company Statcraft started promoting salinity gradient energy (SGE) whilst many researchers from different parts of the world started research for finding ways to enhance the performance of PRO system. Researchers were able to increase the power density from 0.1 Wm^{-2} to 3 Wm^{-2}. The first prototype PRO installation was opened in Norway by Statkraft in 2009. The plant configuration followed the proposed schematic of Loeb and was designed to generate just 10 kW of power, to confirm that the designed system can produce power on a reliable 24 hours per day and as a base for further tests [26].

2.3.6 The 2010s- Present

In 2011, Yip et al. [27] manufactured a thin-film composite (TFC) PRO membrane with a polysulfone (PSF) support layer and a polyamide active layer. In this paper, both internal and external concentration polarization has been considered for developing a prediction model. Yip et al. were able to obtain power density up to 6.1 Wm^{-2}. Since that time, several works have been published on the subject of PRO, studying the parameters to optimize the power density [29–35]. In addition, other interesting PRO projects have been launched, such as “Mega-ton RO-PRO” in Fukuoka City, Japan, and they have started to publish results [7,36]. 30% energy reduction was possible using the SWRO-PRO System in the

"Mega-ton Water System" at mega-ton scale SWRO plants incorporating a 10-inch module prototype PRO plant. The brine disposal problem was also solved by this system [129].

2.4 Pressure Retarded Osmosis Models' Progress

PRO models have been developed and optimized over time. Many researchers utilize modeling of the PRO process in order to gain more insight. The Loeb model, Lee model, Achilli model, Yip model, and Touati model are further described below.

2.4.1 Loeb model

The first model was proposed by Sydney Loeb [13]. Loeb considered that the porous substructure has the character of a boundary layer, in which water flux is a function of the concentrations and the concentration gradients. By considering the salt flux insignificant, he proposed the following model:

$$J_w = A\left(\pi_{Draw} - \pi_{Feed}\exp\left(\frac{\Delta X}{D_{sp}}\right) - \Delta P\right) \quad \text{.....(3)}$$

where π_{Draw} and π_{Feed} and are the osmotic pressures of the draw and feed bulks, respectively, ΔX is the thickness of the membrane, and D_{sp} is the diffusion the coefficient in the support layer.

2.4.2 Lee model

Lee et al [15] proposed a model by considering only internal concentration polarization. He assumed that ECP is greatly reduced by stirring. The equation proposed by Lee et al. for the calculation is as follows:

$$J_w = A\left(\pi_{D,m}\frac{1-\frac{C_{F,b}}{C_{D,m}}\exp(J_w K)}{1+\frac{B}{J_w}[\exp(J_w K-1)]} - \Delta P\right) \quad \text{.....(4)}$$

where $\pi_{D,m}$ is the osmotic pressure at the active layer in the draw bulk side, $C_{F,b}$ and $C_{D,m}$ are, respectively, the concentration of the feed solution and the solute concentration in the active layer of the draw bulk side and K is the solute resistivity.

2.4.3 Achilli Model

Achili et al. [36] modified the model proposed by Lee et al. [15] by considering the ECP phenomenon.

$$J_w = A\left(\pi_{D,b}\exp\left(\frac{-J_w}{k}\right)\frac{1-\frac{\pi_{F,b}}{\pi_{D,b}}\exp(J_wK)\exp\left(\frac{J_w}{k}\right)}{1+\frac{B}{J_w}[\exp(J_wK-1)]}-\Delta P\right)\text{.....(5)}$$

Here k is the mass transfer coefficient.

2.4.4 Yip Model

Yip et al. [27] have further modified the Lee model. Considering the reversal salt flux, he used the following equation for determining the water flux:

$$J_w = A\left(\frac{\pi_{D,b}\exp\left(\frac{-J_w}{k}\right)-\pi_{F,b}\exp\left(J_w\frac{s}{D}\right)}{1+\frac{B}{J_w}\left[\exp\left(\left(J_w\frac{s}{D}\right)-exp\left(\frac{-J_w}{k}\right)\right)\right]}-\Delta P\right)\text{.....(6)}$$

Where s is the structural parameter.

2.4.5 Touati Model

Based on the convection-diffusion theory, Touati et al. [2] developed a model for the water flux as follows:

$$J_w = A\left[\begin{array}{c}\left(\pi_{D,b}+\frac{B}{A}\left(1+\frac{A\Delta P}{J_w}\right)\right)exp\left(\frac{-J_w}{k_D}\right)-\\ \left[\pi_{D,b}+\frac{B}{A}\left(1+\frac{A\Delta P}{J_w}\right)\right]\exp(J_wK)exp\left(\frac{-J_w}{k_F}\right)-\Delta P\end{array}\right]\text{.....(7)}$$

2.5 Pressure Retarded Osmosis Membrane Development

The membrane plays the most crucial role in the overall performance of the pressure retarded osmosis process. Earlier studies have been done using RO membranes concluding the problem associated with RO membrane is severe ICP. This is due to the RO membrane having a thick support layer where salt enters and therefore greatly reducing the effective osmotic driving force. In order to successfully implement the PRO process, development of appropriate membrane is a prerequisite. The following criteria should be satisfied before designing suitable PRO membranes:

- A membrane with high mechanical strength to enhance the overall stability of the process;
- To reduce the effect of ICP, the membrane support layer thickness should be as small as possible. Since salt permeates through the porous support layer, the design support layer porosity should also be taken into consideration; and
- Fouling propensity of the membrane.

Two types of the membrane have been studied so far for the PRO process, namely the flat sheet and hollow fiber membranes.

2.5.1 Flat-sheet membrane

2.5.1.1 Cellulose Acetate Membrane:

In the PRO process, cellulose acetate (CA) is widely used for power generation. It is the most important synthetic cellulose ester. In 1865, it was first produced by cotton anhydrite [37]. The hydrophilic nature of CA has some advantages for the osmotically driven process. Hydrophilicity is desirable as it can increase water flux and reduce membrane fouling, as well as providing good mechanical strength and relatively high tolerance to chlorine [38]. This hydrophilic nature of CA is also responsible for wetting the membrane, hence reducing the ICP [39]. Based on the preferential sorption capillary flow model, Loeb and Sourirajan [40] developed a CA membrane for seawater desalination which promotes the increased use of CA membrane for PRO power generation. In the 1990s, development of Hydration Technology Innovations (HTI) membrane revealed a good performance in PRO bench-scale tests [36]. However, with this conventional CA membrane, Statcraft was able to produce only 1.5 Wm^{-2} power which was far below the targeted 5 Wm^{-2}. Schiestel et al. [41] developed a CA membrane with a better performance than the HTI membrane, with highly porous support layers with a pressure stability up to 20 bars.

2.5.1.2 Thin-Film Composite Membrane

The Thin-Film Composite (TFC) membrane consists of two different types of materials to optimize the performance of both materials. TFC membranes are sensitive to oxidants and chlorine chemicals. Yip et al. [27] first used a PSF-polyamide TFC membrane for a laboratory PRO set up. To give support, a mesh spacer was used. Nano-fiber TFC PRO

membrane was first introduced by Song et al. [42]. The membrane was characterized by an optimized support layer to reduce the effect of ICP**.**

2.5.2 Hollow Fiber Pressure Retarded Osmosis Membrane

A hollow fiber membrane is a tubular, self-supporting membrane with a fiber diameter of less than 500 mm [43]. In a hollow fiber spinning set up, this type of membrane is prepared by applying phase inversion. Chou et al. [44] first used hollow fiber membrane which showed better performance in terms of energy production and mechanical strength compared to the previously used flat sheet membrane. In 2013, Chou et al. [44] introduced another hollow fiber membrane which was also very promising in terms of high energy and mechanical strength. In addition to those added advantages, this modified membrane also showed low reversal salt flux. The hollow fiber membrane used by Chou et al. [44] was modified by polyamide as an active layer and polyetherimide as the substrate layer. Later, several articles have been published on surface modification of the hollow fiber membrane [46–48]. This hollow fiber TFC membrane has high asymmetry and porosity, thick skin layer and narrow pore size distribution underneath the TFC layer which have made it possible to produce a power density of 24.3 Wm^{-2}.

2.6 Draw Solutions

The draw solute plays a very critical role in the successful implementation of the PRO process. Draw solute creates osmotic gradients across semipermeable membranes as the driving force for power generation. Ideally, the semipermeable membrane performs as a barrier that allows only water to pass through but rejects all others. However, in reality, depending on draw solute's chemistry property and physical structure, the reverse flux of draw solutes may take place across the semipermeable membranes which results in a lower effective osmotic driving force and facilitates fouling [48]. Due to the transportation of the draw solute in the support layer, there is a chance of concentration polarization which can eventually be responsible for the low performance of the overall process. Furthermore, the regeneration of draw solutes from diluted draw solutions and the production of clean water might be energy-intensive if inappropriate draw solutes and recycle processes are utilized [48].

Before selecting draw solutes, a few factors should be taken into consideration as the selection of draw solution is very important for the advancement of the PRO process. Appropriate selection of draw solutes can effectively reduce the cost and increase the efficiency of the system. Before the selection of the draw solution, the following criteria should be fulfilled.

Firstly, the draw solute should produce a higher driving force between the two sides of the semipermeable membrane. To maintain a higher driving force, the draw solute should have higher osmotic pressure.

Secondly, the draw solute should have a small reversal salt flux. This is because transportation of solute into the membrane support layer can cause severe concentration polarization. Concentration polarization is found to have one of the most influential drawbacks for the reduction of effective driving force.

Thirdly, the draw solution should be chosen in such a way that it can be regenerated easily. As for closed-loop PRO system, the same draw solution is used repeatedly, so it needs to be regenerated continuously. Usually, closed-loop PRO is coupled with a downstream separation process. Hence, easy regeneration of draw solutions is highly desirable to lower energy consumption and overall operating costs [48].

2.7 Literature review about draw solutions

Research to find better draw solutions for the successful operation of PRO process has recently gained popularity. An overview of various solutes, their recovery methods, and possible drawbacks are summarized in Table 1. From Table 1, it is shown that no comprehensive study (other than sodium propionate) has been studied so far to observe the performance for the PRO process. Therefore, there is a provision for exploring the feasibility of organic draw solution for the performance of closed-loop PRO process.

Table 1 Overview of the used draw solutions for PRO process

Draw solutions			Membrane	Ref.
Name	Conc.	Osmotic pressure (MPa)		
$Na_5[Fe(C_6H_4O_7)_2]$/Water	1 M	-	TFC PRO hollow fiber (Fabricated)	[49]
LiCl/Methanol	1 M	~ 6	TFC PRO hollow fiber (Fabricated)	[49]
NaCl/ DI water	0.6 M	~ 2.76	Flat-sheet cellulose triacetate (CTA) FO membrane (hydration)	[36]
NaCl/ 8.55nM NaCl solution	0.5 M	~ 2.32	Forward osmosis spiral element (HTI OsMem™2521 FO-CTA-MS-P-3H)	[50]
NaCl/ 8.55nM NaCl solution	0.5 M	~ 2.27	Cellulose triacetate (CTA) FO membrane supported by a woven fabric (hydration)	[6]
NaCl/ DI water	1 M	~ 4.88	Flat-sheet cellulose triacetate (CTA) FO membrane (hydration)	[36]
NaCl/ DI water	2 M	~ 10.04	Flat-sheet cellulose triacetate (CTA) FO membrane (hydration)	[51]
$MgSO_4$/Water	1 M	~ 2.6	CA membrane	[52]
$MgCl_2$/Water	0.67	~ 4.85	TFC Membrane	
$MgSO_4$/Water	1 M	~ 2.6	CA membrane	
$MgCl_2$/Water	0.67 M	~ 4.85	TFC Membrane	
$CaCl_2$/Water	1.6 M	-	Commercial Flat-sheet FO membrane (HTI) (Albany, OR)	[53]
HCOONa/Water	4.1 M	-		
KBr/Water	3.2 M	-		
LiBr/Water	2.2 M	-		
LiCl/Water	2.6 M	-		
$Na(C_2H_5COO)$ /Water	4.1 M	-		
LiCl/Methanol	3 M	-	Commercial thin-film composite (TFC) membrane, (HTI, Albany, OR),	[54]

2.8 Membrane Distillation process (MD)

Membrane distillation (MD) is a thermally driven separation process. A hydrophobic membrane displays a barrier for the liquid phase, allowing the vapor phase

(e.g. water vapor) to pass through the membrane's pores. The driving force of the process is given by a partial vapor pressure difference commonly triggered by a temperature difference [55].

2.9 Utilization of low-grade waste heat

Utilization of low-grade waste heat is very crucial for the optimal operation of closed-loop PRO system. During the industrial manufacturing processes, 20 to 50% of the energy consumed is ultimately lost via waste heat contained in streams of hot exhaust gases and liquids, as well as through heat conduction, convection, and radiation from hot equipment surfaces and from heated product streams[56]. Therefore, the closed-loop PRO process can be co-located with existing power plants such as traditional and geothermal power plants, or other industrial processes that emit low-grade heat such as chemical processing plants, cement plants, and breweries. During the closed-loop PRO process, thermal and membrane distillation processes can be used to regenerate thermolytic and distillable draw solutes, respectively, using industrial waste heat. Utilization of solar panel wasted heat can be another potential aspect of closed-loop PRO as around 60-94% energy is lost from the solar panel as waste heat. If closed-loop PRO can be properly incorporated into the existing solar panel, it could sufficiently raise the temperature of the PRO section and MD can be successfully operated.

Chapter 3: Highly Effective Organic Draw Solutions for Renewable Power Generation by Closed-Loop Pressure Retarded Osmosis

3.1 Introduction

Increasing rates of global energy use are diminishing the existing fossil fuel reserves. To secure a sustainable future for ourselves and generations to follow, it is widely accepted that we must act now to produce renewable energy. In light of this challenge, a massive amount of research is being conducted about the use of clean, renewable energy sources [58–66]. Pressure retarded osmosis is known as an emerging technology for renewable energy [66]. PRO is an osmotically driven membrane-based process that harnesses the energy gradient between high and low salinity streams to produce mechanical energy [14]. The primary concept behind this process is the osmotic transport of water through a semi-permeable membrane from a low salinity feed solution into a high salinity draw solution. This approach utilizes the natural process of osmosis, which is the diffusion of salt due to different salinities on either side of a semi-permeable membrane. During the PRO process, a pressure that is lower than the osmotic pressure is applied to the draw solution side to generate electricity via a turbine-generator, which is set by releasing a portion of the pressured water that permeates across the membrane from the low salinity solution [36-37,45,52,68]. PRO processes can be classified into two types: open-loop PRO and closed-loop PRO processes. The diluted draw solution is discharged during the open-loop PRO process, whereas the draw solution with osmotic potential is regenerated instead of discharged during the closed-loop PRO process [37]. The closed-loop PRO process consists of three sections, that is, the PRO filtration unit, hydro turbine and draw solution regeneration system. A schematic representation of a closed-loop PRO is shown in Figure 5.

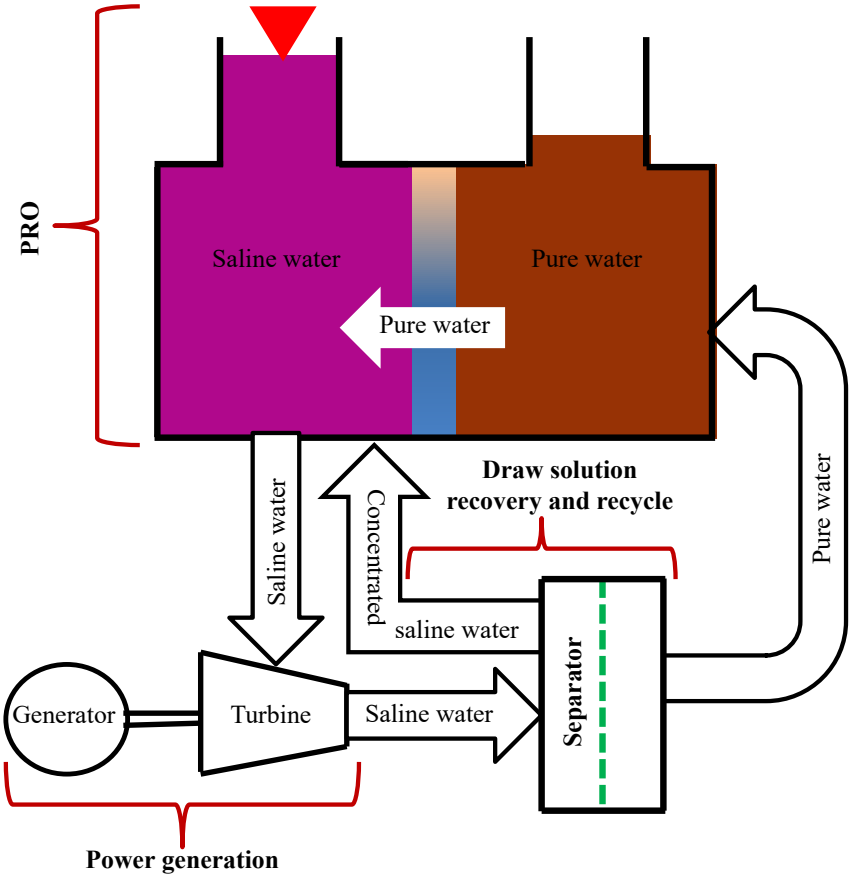

Figure 5 A schematic representation of the closed-loop PRO process

A closed-loop PRO process can be economically viable when the minimum peak power density value is approximately 5.0 W/m^2 [69–72]. Low-grade industrial heat can be used to regenerate the draw solution within the closed-loop PRO process [72]. During the industrial processes, 20–50% of the consumed energy is lost as waste heat in the form of hot exhaust gasses, cooling water, and radiant heat from hot equipment surfaces and other heated products [53]. Therefore, the closed-loop PRO process can be co-located with existing power plants, such as traditional and geothermal power plants or other industrial processes that emit low-grade heat, such as chemical processing plants, cement plants, and breweries. During the closed-loop PRO process, thermal and membrane distillation processes can be used to regenerate thermolytic and distillable draw solutes, respectively, using industrial waste heat [54,73-74]. The above context makes the closed-loop PRO process an appropriate emerging technology for the production of renewable energy from

the salinity gradient of two solutions that are separated by a semi-permeable membrane [8,54,73–75].

The efficiency of the PRO process is highly dependent on the membrane, the draw solution used, the recovery system chosen and the power density obtained for electricity generation [8,36–38,45,52–54,73–75]. In recent years, various inorganic salts have been used as draw solutions in membrane-based osmotic processes in which high reverse salt fluxes were observed [53,76–79]. Draw solutions with high solubility and high osmotic pressure yet lower reverse salt flux is most effective for membrane-based osmotic processes [53,76–79]. Previously, Hickenbottom et al., Bowden et al. and Corzo et al. used organic draw solutions in membrane-based osmotic processes [54,80,81]. Compared to inorganic draw solutions, some of the tested organic draw solutions exhibited high solubility and high osmotic pressure, but more importantly, all of those organic draw solutions studied possessed lower reverse salt fluxes [76–81]. The low reverse salt flux of draw solutions can decrease concentration polarization, which is required to achieve high water flux in the membrane-based osmotic processes [53-54,76–82]. High water flux contributes to provide high power density in PRO [8,53-54,74-75]. Therefore, in the search for effective organic draw solutions for renewable power generation via PRO, we—for the first time—report eleven organic draw solutions (potassium citrate, calcium acetate, potassium oxalate, potassium acetate, ammonium acetate, ammonium carbamate, ammonium formate, potassium formate, sodium glycolate, sodium propionate, and calcium propionate) with high solubility, high osmotic pressure, tangible feasibility for recovery by low temperature thermal distillation/membrane distillation, very low reverse salt flux and viability for power generation.

3.2 Selection of organic draw solutions

Figure 6 represents the method used to select organic draw solutions. Initially, 550 organic compounds were screened as potential draw solutions. The compounds that were not solid at normal temperature and pressure and not soluble in water were eliminated by the database-driven screening method to create a short list of potential chemicals. The osmotic pressures of the draw solutions as a function of the concentration were then determined

using the OLI Stream Analyzer™ (OLI Systems, Inc.). Draw solutions with an osmotic pressure lower than 2.8 MPa, the osmotic pressure of seawater [76], at the saturation concentration were excluded to obtain the desired draw solutes. At the end of the selection process, the following eleven organic compounds were identified as desirable organic draw solutes: potassium citrate, calcium acetate, potassium oxalate, potassium acetate, ammonium acetate, ammonium carbamate, ammonium formate, potassium formate, sodium glycolate, sodium propionate, and calcium propionate.

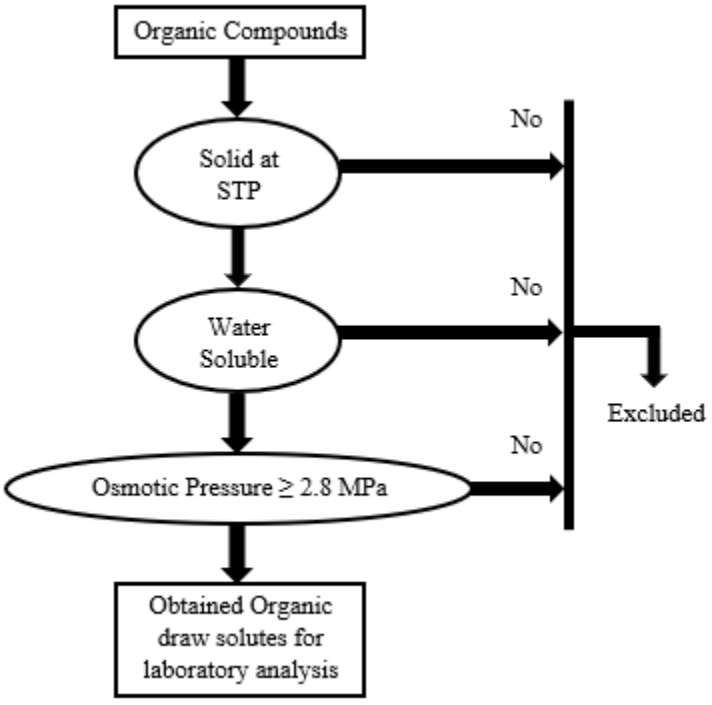

Figure 6 Flow chart for the selection of the organic draw solutes

3.3 Materials and Experimental Methods

3.3.1 Solution of the draw solutes

Certified ACS-grade organic compounds from Sigma-Aldrich, USA were used to produce all the draw solutions. These draw solutions are all provided in Table 2. De-ionized (DI) water (Millipore, Billerica, MA) was used as the feed stream in the experiments. The concentrations of each draw solution at 2.8 and 4.2 MPa osmotic pressure were determined

using the OLI Stream Analyzer™ (OLI Systems, Inc.) (Table 2). The OLI Stream Analyzer™ was also used to find the mutual diffusivity (D), viscosity, and solubility for each draw solution (Table 2).

Table 2 Properties of the draw solutions at a temperature of 24 °C.

Draw solution	D ($\times 10^{-9}$ m^2/s)	At 2.8 MPa osmotic pressure			Solubility (g/L)	Conc. (M) at solubility	Osmotic pressure (MPa) at solubility	Viscosity (cP) at solubility
		Conc. (g/L)	Conc. (M)	Viscosity (mPa.s)				
Potassium citrate (KCit)	0.7197	134.81	0.42	0.98	649	2.0	13	7.12
Calcium acetate (CaAc)	0.7948	129.70	0.82	0.99	347	2.19	7	4.24
Potassium oxalate (KOxa)	0.850	66.00	0.36	1.00	377	2.05	15.30	8.66
Potassium acetate (KAc)	0.9873	64.80	0.66	1.02	2570	26.19	108	59.9
Ammonium acetate (NH_4Ac)	1.155	70.14	0.91	1.00	1430	18.55	33.10	33.23
Ammonium carbamate (NH_4C)	1.250	30.04	0.38	0.98	580	6.60	45.20	26.72
Ammonium formate (NH_4F)	1.322	39.30	0.62	1.03	1427	22.63	101	61.66
Potassium formate (KF)	1.3477	57.20	0.68	1.00	2713.60	32.26	130	74.96
Sodium glycolate (NaGly)	1.547	72.05	0.73	1.04	650	6.56	24.60	16.26
Sodium propionate (NaP)	1.643	66.30	0.69	0.98	1000	10.41	41.80	26.61
Calcium propionate (CaP)	1.708	108.00	0.58	1.02	503.60	2.70	13	8.07
Sodium chloride (NaCl)	1.38	35.40	0.61	0.99	359	6.14	27.40	25.13
Ammonium bicarbonate (NH_4HCO_3)	1.42	52.90	0.67	1.01	220	2.78	11.50	6.72

3.3.2 Membrane performance evaluation

A flat-sheet of TFC forward osmosis membrane (Hydration Technology Innovations, HTI, Albany, OR) was used to conduct all PRO experiments. The water permeability coefficient (A) and salt permeability coefficient (B) for the TFC membrane was investigated using a flat-sheet bench-scale cross-flow reverse osmosis (RO) test system. A coupon of the membrane with an effective surface area of 19.94 cm^2 was placed in a stainless steel test cell with an active surface of the membrane facing the feed stream. The membrane coupon was also placed in the stainless steel test cell with the support surface of the membrane facing the feed stream in order to investigate water permeability coefficient. Using a high-pressure positive displacement pump (Hydra-cell pump), the feed solution was re-circulated at 1.0 L/min. DI water was used as the feed stream to investigate A and a 20 mM solution of each draw solute was used as the feed stream to investigate salt rejection (R) and B for the TFC membrane.

The A, R, and B for the membrane were determined using the following equations [47,50, 83-84]:

$$J = \frac{\Delta V}{A_m \Delta t} \quad \text{.....(8)}$$

$$A = \frac{J}{\Delta P} \quad \text{.....(9)}$$

$$R\,(\%) = \frac{C_f - C_p}{C_f} \times 100 \quad \text{.....(10)}$$

$$B = \frac{A(1-R)(\Delta P - \Delta \pi)}{R} \quad \text{.....(11)}$$

where J is the pure water flux, A_m is the effective membrane area, ΔV is the permeate volume, Δt is time, ΔP is the hydraulic pressure difference across the membrane, C_f is the salt concentration of the feed solution, C_p is the salt concentration of the permeate solution and $\Delta\pi$ is the osmotic pressure of the feed solution.

The pressure was increased in 0.345 MPa incrementally from 0.345 to 1.034 MPa to investigate the A of the TFC membrane. Constant pressure was applied at each increment for 8 hours. The water flux through the membrane was obtained from a liquid flow sensor (Sensirion, The Sensor Company) that was directly connected to a computer. To investigate R and B, 1.896 MPa of pressure was applied to the RO cell. The salt concentration of the permeate solution was

investigated using a calibrated conductivity meter (Oakton, Eutech Instruments). This experiment was conducted at a constant temperature of 24 °C using a chiller (Polystat, Cole-Parmer).

A flat-sheet bench-scale FO test system in PRO mode was used to determine the structural parameter (S) of the TFC membrane by applying the following equation [12,83–85]. De-ionized water was used as the feed solution, while a concentration of all draw solutions at a 2.8 MPa osmotic pressure was used.

$$S = \left(\frac{D}{J_w}\right) \ln\left[\frac{A\,\pi_{draw} - J_w + B}{A\,\pi_{feed} + B}\right] \quad \text{.....(12)}$$

where J_w is the FO water flux (PRO mode) for the draw solutions.

3.4 PRO experiment for the draw solutions

The bench-scale PRO experimental setup is presented in Figure 14. A coupon of the membrane with an effective surface area of 19.94 cm^2 was placed in a cross-flow cell with the active layer of the membrane facing the draw stream. Tricot spacers were used in both the feed and draw channels to support the membranes under the high applied pressures. The feed and the draw solutions were circulated in a closed-loop system using a variable speed gear pump (Cole-Parmer Instrument Company) and a high-pressure pump (Hydra-cell pump), respectively. A backpressure valve was installed at the outlet on the draw side with a bypass valve connected to the high-pressure pump. These two valves controlled the flow rate of the solution and the inlet draw pressure. Chillers were used to maintain a constant temperature of 24 °C for the feed solution and draw solution. The water flux for the draw solution was obtained by measuring the weight of the feed solution with a digital analytical balance. Solutions of KCit (0.42 M and 0.62 M), CaAc (0.82 M and 1.22 M), KOxa (0.36 M and 0.55 M), KAc (0.66 M and 0.97 M), NH_4Ac (0.91 M and 1.32 M), NH_4C (0.38 M and 0.58 M), NH_4F (0.62 M and 0.91 M), KF (0.68 M and 0.99 M), NaGly (0.73 M and 1.07 M), NaP (0.69 M and 1.01 M), CaP (0.58 M and 0.87 M), NaCl (0.61 M and 0.93 M) and NH_4HCO_3 (0.67 M and 1.03 M) in DI water were used as draw solutions, where only DI water was used as the feed solution for the PRO experiments. The flow rate of the feed side was maintained at a constant 0.8 L/min, whereas that of the draw side gradually increased from 0.5 L/min to 0.8 L/min, depending on the applied pressure. The draw side was pressurized to 1.8 MPa (for 2.8 MPa osmotic pressure of the draw solutions) at increments of 0.2 MPa at each stage. The draw side was

pressurized to 2.1 MPa for 4.2 MPa osmotic pressure for the draw solutions. Once the system was stabilized, the membranes were tested for 30 min at each pressure point before moving to the next one. The DI feed water was held in a 4 L constant-level reservoir. The draw solution was contained in another 4 L reservoir. The water flux was determined to evaluate the PRO performance for each draw solution. The water flux of the draw solution was obtained from a digital [85] analytical balance using equation (8). To investigate the reverse salt flux, a sample of the feed solution was collected before and after the experiment to determine the salt concentration using a calibrated conductivity meter (Oakton, Eutech Instruments). The reversal salt flux was calculated by using the following equation [86]:

$$J_s = \frac{C_f V_f - C_{f,i} V_{f,i}}{A_m \Delta t} \quad \text{.....(13)}$$

where C_f and V_f are the salt concentration and total volume of the feed at the end of the tests, respectively, and $C_{f,i}$ and $V_{f,i}$ are the initial salt concentration and the total volume of the feed, respectively.

3.5 Investigation of the thermolytic and thermally distillable properties of the draw solutes

The thermolytic and thermally distillable properties of the draw solutes were investigated using the gravimetric method. For this method, the fixed weight (W_1 g) of a draw solute was collected. A solution of the draw solute was then prepared with DI water. The draw solution in a beaker (liquid surface area 18.09 cm^2) was heated at 50 °C to evaporate all the water, and then the residue was weighed (W_2 g).

If $W_1 = W_2$, the draw solute is distillable.

If $W_1 > W_2$, the draw solute is thermolytic.

Afterward, the osmotic pressures of the distillable draw solute residues were investigated using a Micro-Osmometer (Precision Systems) at 24 °C. The Micro-Osmometer was used to determine the osmolality (Osmol/kg) of each draw solution. The osmolality was then converted to molality (mol/kg) for each draw solution. Finally, the following equation was used to calculate the osmotic pressure [51]:

$$\pi = \rho R_1 Tm \quad \text{.....(14)}$$

where π is the osmotic pressure, ρ is the density of the solvent (water), R_1 is the gas constant, T is the absolute temperature, and m is the molality.

3.6 Results and Discussion

3.6.1 Water permeability and structural parameters of the membrane

The cross-flow RO cell used to investigate the pure water permeability of the commercial TFC membrane found a membrane water permeability value of 32.5 LMH/MPa. This water permeability value is very close to the value of 31.6 LMH/MPa reported in the literature for the same type of membrane [87]. The structural parameters of the membrane for all the draw solutions were determined by investigating the salt rejection and salt permeability coefficient in a cross-flow RO cell, with results shown in Table 3. The salt rejection for the organic draw solutions was 99.43% – 99.65%, whereas it was 97.27% and 96.64% for NaCl and NH_4HCO_3, respectively. The salt permeability coefficient of the organic draw solutions was 0.202 LMH – 0.340 LMH, which was much lower than the compared NaCl and NH_4HCO_3 draw solutions at1.65 LMH for NaCl and 2.05 LMH for NH_4HCO_3. Higher salt rejection and lower salt permeability coefficients were obtained for the organic draw solutions due to the larger sizes of their hydrated ions compared to that of the NaCl and NH_4HCO_3 draw solutions. The Forward Osmosis (FO) water flux for the draw solutions at 2.8 MPa osmotic pressure in PRO mode against DI water are presented in Table 3. The FO water flux obtained in PRO mode for the organic draw solutions, excluding KCit, found in the range of 25.96 LMH to 39.50 LPH were higher than those of the NaCl at 24.89 LMH and NH_4HCO_3 at 23.67 LMH draw solutions when measured at the same osmotic pressure (2.8 MPa). Higher water fluxes for the organic draw solutions were likely obtained due to the much lower salt permeability compared to NaCl and NH_4HCO_3. The FO water fluxes in PRO mode for the NaCl and NH_4HCO_3 draw solutions when using the same type of membrane, measured at ~38 LMH for NaCl and ~36 LMH for NH_4HCO_3 draw solutions at 1 M concentration each, are comparable to the literature reported values) [87]. In our experiments, the concentrations of the NaCl and NH_4HCO_3 draw solutions, measured at 0.61 M for NaCl and 0.67 M for NH_4HCO_3, were lower (0.61 M) than values found in literature. Consequently, the water fluxes obtained for the NaCl and NH_4HCO_3 draw solutions in our experiments were lower compared to the values reported in the

literature [87]. The structural parameter of the membrane for the organic draw solutions ranged from 615 to 802 µm, which were comparable to the values for the NaCl and NH_4CO_3 draw solutions, measured at 742 µm and 761 µm, respectively.

Table 3 Structural parameter of the membrane.

Draw solution	Conc. (mM)	Osmotic pressure (MPa)	R (%)	B (LMH)	FO water flux (LMH) in PRO mode	S (µm)
KCit	20	0.13	99.65	0.202	22.93	658
CaAc		0.07	99.63	0.220	25.96	627
KOxa		0.16	99.60	0.227	28.00	615
KAc		0.08	99.58	0.249	30.65	637
NH_4Ac		0.04	99.56	0.266	31.40	715
NH_4C		0.15	99.55	0.257	32.78	744
NH_4F		0.09	99.45	0.324	33.50	736
KF		0.08	99.43	0.340	33.96	734
NaGly		0.08	99.52	0.285	36.58	799
NaP		0.08	99.51	0.291	39.03	790
CaP		0.10	99.50	0.293	39.50	802
NaCl		0.09	97.27	1.65	24.89	742
NH_4HCO_3		0.08	96.64	2.05	23.67	761

***** Applied pressure for the rejection test in the RO experiment was 1.896 MPa.

3.6.2 Reverse salt flux of the draw solutions in the PRO process

The reverse salt fluxes of the draw solutions in the PRO process are shown in Figure 7A and Figure 7B. The reverse salt fluxes of the organic draw solutions at the osmotic and applied pressures of 2.8 MPa and 0.2 MPa, respectively, ranged from 0.0272 mol m^{-2} h^{-1} to 0.068 mol m^{-2} h^{-1} (Figure 7A). The reverse salt fluxes were almost identical at applied pressures of 0.2 MPa and 1.4 MPa (Figure 7A) for each organic draw solution at the same osmotic pressure = (reverse salt flux 0.029 mol m^{-2} h^{-1} to 0.0699 mol m^{-2} h^{-1} at osmotic and applied pressures of 2.8 MPa and 1.4 MPa, respectively, for the organic draw solutions). During the membrane-based osmotic processes, the reverse salt flux is substantially influenced by the diffusivity of the draw solutions, shown when a higher reverse salt flux is obtained for the draw solutions with higher diffusivity values [3]. For our selected organic draw solutions, a higher reversal salt flux was obtained for all draw solutions with higher mutual diffusivity (Table 2 and Figure 7A), excluding the NH_4F and KF draw solutions. Both the mutual diffusivity and hydrated anion sizes could affect the reverse salt flux

for these two draw solutions. In fact, the draw solutions with higher diffusivity values demonstrated a higher driving force that helped the draw solute to pass through the membrane. The higher diffusivity of a draw solution means that the draw solute can move quickly in the solution from a high concentration area to a low concentration area. The driving force means the force that can promote solute movement in the solution from a high concentration area to a low concentration area. Thus, the draw solution with a higher diffusivity can achieve a higher driving force, which can promote the passage of the draw solute through the membrane from the draw side (high concentration area) to the feed side (low concentration area). The reverse salt flux of all the organic draw solutions was almost constant as a function of increasing pressure during the PRO process. Compared to the inorganic draw solutions (NaCl and NH_4HCO_3), the reverse salt fluxes of the selected organic draw solutions were much lower under the same experimental conditions (Figure 7A and Figure 7B). The reverse salt flux of NaCl and NH_4HCO_3 draw solutions at 0.2 MPa of applied pressure were 0.257 mol m^{-2} h^{-1} and 0.2993 mol m^{-2} h^{-1}, respectively (Figure 7B). These reverse salt fluxes for the NaCl and NH_4HCO_3 draw solutions are similar to the literature reported values of0.38 mol m^{-2} h^{-1} for NaCl and 0.54 mol m^{-2} $h^{-1}$for NH_4HCO_3 at 1 M draw solution while using the same type of membrane [87]. The reverse salt fluxes for these two draw solutions were lower compared to the literature-reported values because lower concentrations of NaCl (0.61 M) and NH_4HCO_3 (0.67 M) solutions were used in our experiments. The reverse salt flux also increased with increasing pressure for the NaCl and NH_4HCO_3 draw solutions during the PRO process. In fact, the draw solutions containing larger-sized hydrated anions show lower reverse salt fluxes [76]. All the anions in the organic draw solutes contain a C-O double bond, which can be polarized, especially the π-bond of the double bond, in their aqueous solutions (Figure 7C). This polarizing nature promotes the hydration of the organic draw solutes with more water molecules compared to the chloride ion (Cl^-). Hence, the sizes of the hydrated anions in the organic draw solutes were larger than they were in the Cl^- ions.

Citrate and oxalate ions contain a larger number of C-O double bonds (3 double bonds for citrate and 2 double bonds for oxalate) and negative charges (3 negative charges for citrate and 2 negative charges for oxalate) when compared to bicarbonate ions (bicarbonate ion contains one C-O double bond and one polar O-H bond), as shown in Table 4. Due to the larger number of double bonds and negative charges, more citrate and oxalate ions were hydrated with water molecules, producing larger-sized hydrated anions compared to the bicarbonate ion. While the bicarbonate ion contains

one C-O double bond and one polar O-H bond, carbamate ion contains one C-O double bond with two polar N-H bonds and the glycolate ion contains one C-O double bond with one O-H polar bond-adjacent bulky methylene group (-CH_2-) (Table 4). The characteristics of carbamate and glycolate ions produced larger hydrated anions in comparison with the bicarbonate ion in their respective aqueous solutions. The propionate and acetate ions contain bulky ethyl (-C_2H_5) and methyl (-CH_3) groups, respectively, which are not present in the bicarbonate ion (Table 4). However, these three ions contain the same number of C-O double bonds (one C-O double bond). The presence of bulky groups in propionate and acetate ions produced significantly larger-sized hydrated anions compared to bicarbonate ion.

A higher reverse salt flux was obtained for bicarbonate ion when compared to the formate ion. This finding can be explained by the respective stabilities of these two ions. The lone pair electrons of oxygen atom available between the H and C atoms in the hydrated bicarbonate ion can take part in resonance, whereas no resonance can occur in the formate ion due to the absence of an oxygen atom between the H and C atoms. Due to resonance, unstable charges might form in the bicarbonate ion, making it unable to form stable hydrated anions. The higher salt permeability of the NaCl and NH_4HCO_3 draw solutions in the RO test (Table 3) supports the higher reverse salt flux compared to the selected organic draw solutions in the PRO test.

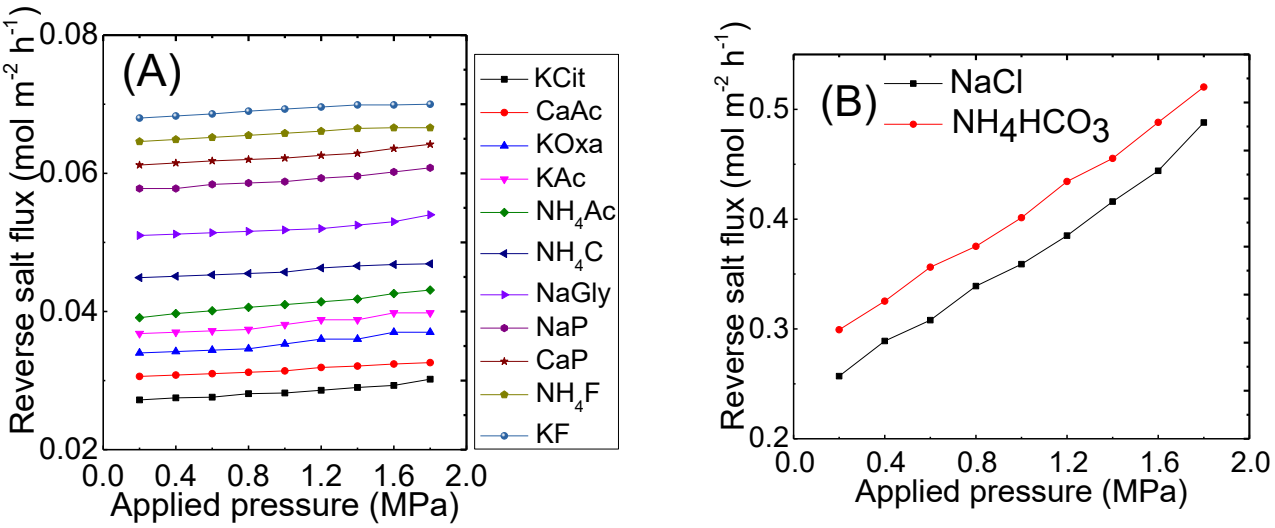

Figure 7 (A) Reverse salt flux of the organic draw solutions (B) and the draw solutions of NaCl and NH_4HCO_3 at various applied pressures during the PRO tests

Table 4 Structural formulas for anions of the draw solutes

Anion name	Structural formula	
Chloride	Cl^-	Inorganic
Bicarbonate	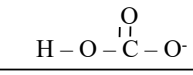	
Citrate	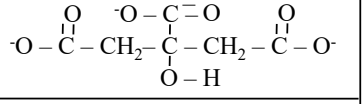	Organic
Oxalate	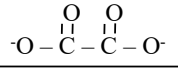	
Carbamate	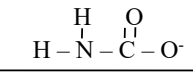	
Glycolate	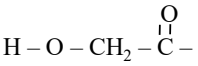	
Propionate	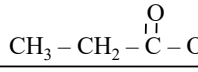	
Acetate	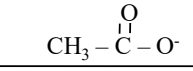	
Formate	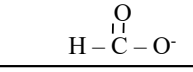	

3.7 Water flux and power density of the draw solutions during the PRO process

The higher value of the mutual diffusivity enhances the diffusion rate of the draw solute in solution. This higher diffusion rate can increase the solute concentration on the active layer (for the depletion of the external concentration polarization), which can generate a higher concentration gradient between the feed solution and the draw solution. By contrast, the higher diffusion rate can increase the reverse salt flux (leading to the development of internal concentration polarization), which can reduce the concentration gradient between the feed solution and the draw solution. Hence, the draw solution with a high diffusion rate and low reverse salt flux can provide a high water flux. The water flux and power density are directly proportional at a constant applied pressure during the PRO process [88]. The water flux and power density calculated by Eq. (2) as a function of the applied pressure for the organic draw solutions and the inorganic draw solutions (NaCl and NH_4HCO_3). The highest and lowest water flux were obtained for CaP (17.30 LMH) and

KCit (13.68 LMH), respectively, at the applied pressure of 1.4 MPa (applied pressure at peak power density for 2.8 MPa osmotic pressure of draw solutions) (Figure 8A). The highest and lowest water flux values were obtained due to the highest and lowest values of mutual diffusivities for the CaP and KCit draw solutions. These parameters also give a very low reverse salt flux (Table 2 and Figure 7). The water flux for the organic draw solutions decreased as a function of increasing applied pressure. This trend is due to an increase in the liquid hydrostatic forces in the draw solution side. The power densities of the organic draw solutions increased with increasing applied pressure (Figure 8B). The maximum power density (peak power density, W_{max}) of the organic draw solutions was obtained at an applied pressure of 1.4 MPa, which was half the osmotic pressure of the draw solutions. The peak power density of the identified organic draw solutions ranged from 5.32 W/m^2 to 6.73 W/m^2 (KCit 5.32 W/m^2, CaAc 5.73 W/m^2, KOxa 5.93 W/m^2, KAc 6.02 W/m^2, NH_4Ac 6.16 W/m^2, NH_4C 6.36 W/m^2, NH_4F 6.43 W/m^2, KF 6.47 W/m^2, NaGly 6.65 W/m^2 , NaP 6.71 W/m^2 and CaP 6.73 W/m^2). At an applied pressure of 0.2 MPa, the water fluxes for NaCl (22.51 LMH) and NH_4HCO_3 (21.27 LMH) were relatively low when compared to the

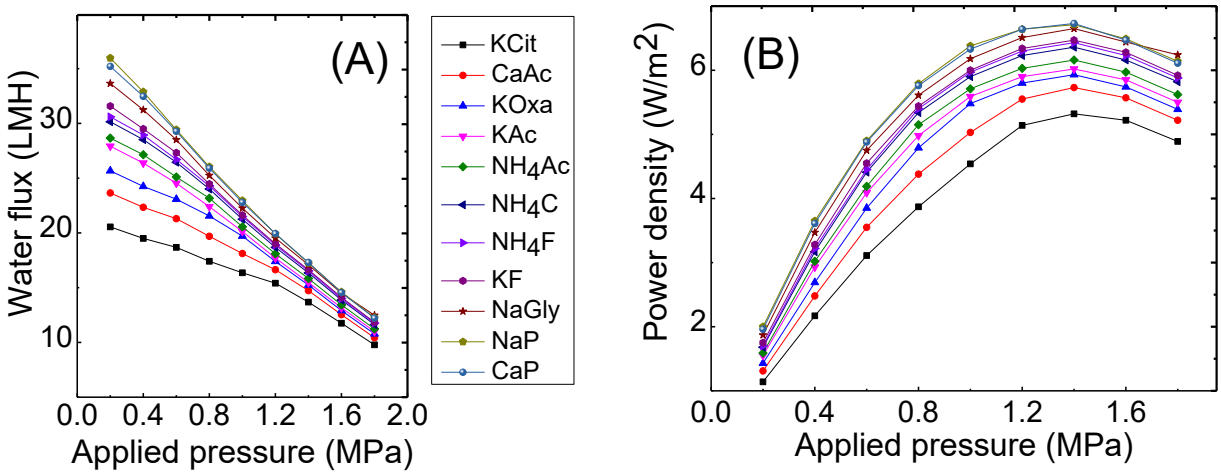

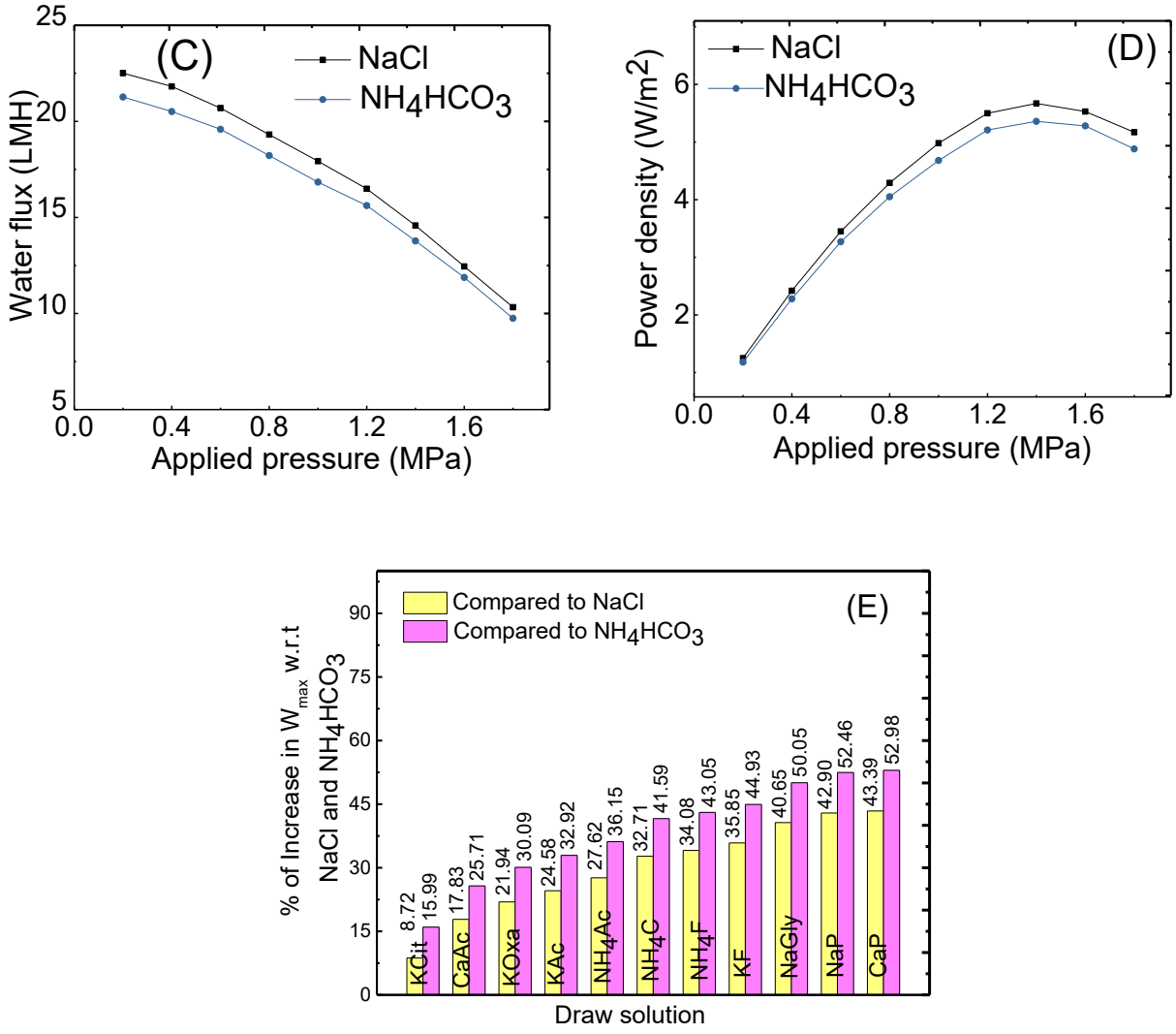

Figure 8 Water flux and power density as a function of the applied hydraulic pressure for the organic draw solutions (A, B) and for the draw solutions of NaCl and NH_4HCO_3 (C, D) at an osmotic pressure of 2.8 MPa, and (E) the percentage of higher peak power density

organic draw solutions (except KCit) due to the increased reverse salt flux for NaCl and NH_4HCO_3 (Figure 8A and figure 8C). The water flux for the inorganic draw solution decreased with increasing applied pressure, similar in response to the organic draw solutions. The obtained peak power densities for the NaCl and NH_4HCO_3 draw solutions were 5.67 W/m^2 and 5.36 W/m^2, respectively (Figure 8D), which were lower than that of the organic draw solutions (excluding KCit at 5.32 W/m^2). The peak power density of the organic draw solutions at the osmotic pressure of 2.8 MPa was higher by -6.17% to 18.69% and -0.75% to 25.56% when compared to NaCl and

NH_4HCO_3, respectively (Figure 8E). The peak power density of the draw solutions was also investigated at an osmotic pressure of 4.2 MPa. The draw solution concentrations at 4.2 MPa osmotic pressure were higher than those of the osmotic pressure of 2.8 MPa (Table 2 and Table 5). The concentrations and the corresponding viscosities of the draw solutions at the osmotic pressure of 4.2 MPa are presented in Table 5.

Table 5 Concentration and viscosity of the draw solutions at 4.2 MPa osmotic pressure

Draw solutions	At 4.2 MPa osmotic pressure	
	Conc. (M)	Viscosity (cP)
KCit	0.62	1.03
CaAc	1.22	1.05
KOxa	0.55	1.02
KAc	0.97	1.04
NH_4Ac	1.32	1.06
NH_4C	0.58	1.02
NH_4F	0.91	1.05
KF	0.99	1.03
NaGly	1.07	1.07
NaP	1.01	1.01
CaP	0.87	1.05
NaCl	0.93	1.03
NH_4HCO_3	1.03	1.05

The reverse salt flux of the organic draw solutions ranged from 0.0325 mol m^{-2} h^{-1} to 0.0854 mol m^{-2} h^{-1}, while it was significantly higher for NaCl (0.854 mol m^{-2} h^{-1}) and NH_4HCO_3 (0.952 mol m^{-2} h^{-1}) at the osmotic pressure and at applied pressure of 4.2 and 2.1 MPa, respectively (Figure 9A). The reverse salt flux of the NaCl and NH_4HCO_3 draw solutions increased alongside the increasing osmotic pressure and concentration (from 2.8 MPa to 4.2 MPa osmotic pressure) (Figure 7B and Figure 9A). The organic draw solutions, however, remained similar at osmotic pressures of 2.8 MPa and 4.2 MPa (Figure 7A and Figure 9A) due to the larger sizes of the organic molecules.

The water fluxes achieved for the organic draw solutions were higher than those of NaCl and NH_4HCO_3 (Figure 9B). The water fluxes obtained for the organic draw solutions were 19.02 LMH to 25.09 LMH, whereas the water fluxes of 17.50 LMH for NaCl and 16.40 LMH for NH_4HCO_3 were obtained at osmotic and applied pressures of 4.2 MPa and 2.1 MPa, respectively. In fact, the high reverse salt flux generated a polarization that prevented desirable water fluxes for the NaCl and NH_4HCO_3 draw solutions. The higher water fluxes for the organic draw solutions produced

higher peak power density (W_{max}), which were calculated using Eq. (2) yielded values of 11.10 W/m^2 to 14.64 W/m^2, compared to NaCl (10.21 W/m^2) and NH_4HCO_3 (9.57 W/m^2) (Figure 9B). The peak power density values of the organic draw solutions at an osmotic pressure of 4.2 MPa were 8.7% to 43.4% and 16% to 53% higher compared to NaCl and NH_4HCO_3, respectively (Figure 9C).

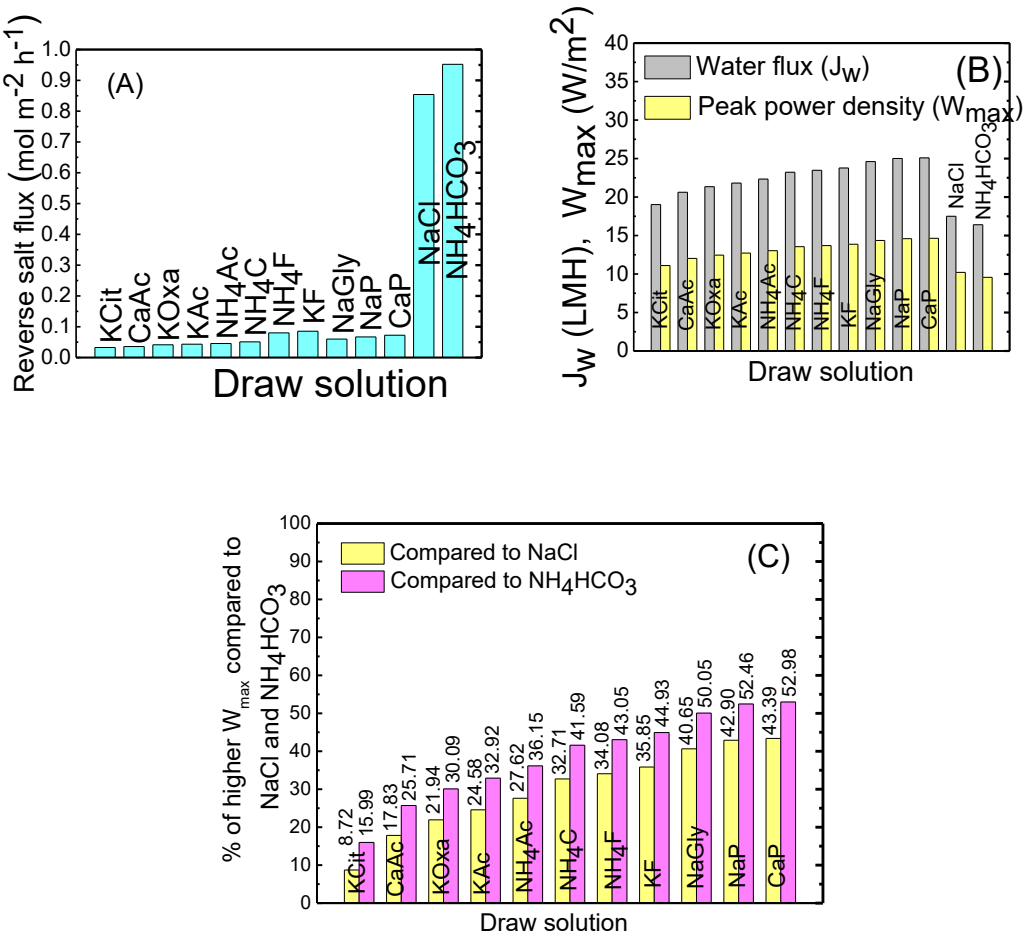

Figure 9 (A) Reverse salt flux and (B) the water flux and peak power density of the draw solutions at 4.2 MPa osmotic pressure with an applied pressure of 2.1 MPa, and (C) the percentage of higher peak power densities in the organic draw solutions compared to the NaCl and NH_4CO_3 draw solutions at the osmotic pressure of 4.2 MPa

The incremental peak power density of the draw solution from 2.8 MPa to 4.2 MPa osmotic pressure is presented in Figure 10. A peak power density increase of 109% to 118% (KCit 109%, CaAc 110%, KOxa 110%, KAc 111%, NH_4Ac 112%, NH_4C 113%, NH_4F 113%, KF 114%, NaGly

116%, NaP 117% and CaP 118%) for organic draw solutions, and an 80% peak power density for NaCl and 79% for NH_4HCO_3 was achieved when increasing the osmotic pressure from 2.8 MPa to 4.2 MPa. The lower peak power density for the NaCl and NH_4HCO_3 draw solutions was produced due to their higher reverse salt flux and higher concentration polarization compared to the organic draw solutions.

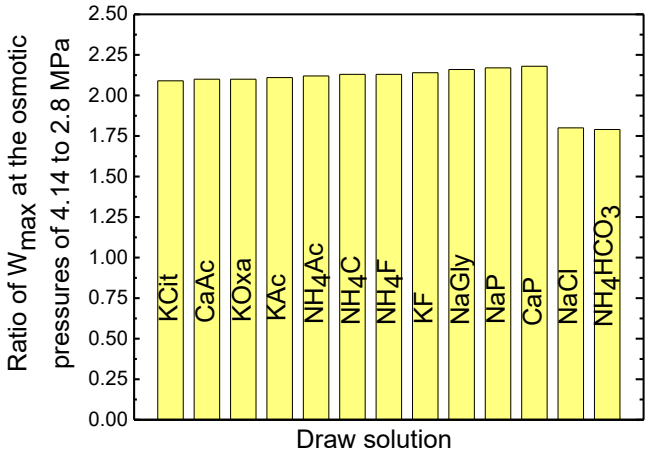

Figure 10 Increment (times) of peak power density at 4.2 MPa from 2.8 MPa osmotic pressure for the draw solutions

The highest osmotic pressure of the selected organic draw solutions ranged from 13 MPa to 130 MPa (excluding CaAc 7 MPa), while it peaked at 27.4 MPa for NaCl and 11.5 MPa for NH_4HCO_3 (Table 2). As discussed above, the reverse salt flux for the NaCl and NH_4HCO_3 draw solutions is much higher at 4.2 MPa osmotic pressure than that at 2.8 MPa osmotic pressure. This tendency indicates an increase of reverse salt flux with increasing osmotic pressures past 4.2 MPa. This high reverse salt flux will generate high concentration polarization, which will prevent the achievement of desirable water fluxes for the NaCl and NH_4HCO_3 draw solutions.

The reverse salt flux for the organic draw solutions was similar at osmotic pressures of 2.8 MPa and 4.2 MPa, which indicates further osmotic pressure and concentration change will not generate concentration polarization effects. Hence, desirable water fluxes were achieved for organic draw solutions at 4.2 MPa osmotic pressure. Due to the low reverse salt flux (maximum 0.0525 mol m^{-2} h^{-1}) trend, the organic draw solutions can be effectively used at osmotic pressures higher than 4.2

MPa. Thus, the selected organic draw solutions, in comparison to NaCl and NH_4HCO_3, would be able to provide a much higher water flux/peak power density at high osmotic pressures.

The osmotic pressures of the identified organic draw solutions at their solubility are 7 MPa to 130 MPa (Table 2). The peak power density for any draw solution is obtained at the applied hydraulic pressure equal to half the osmotic pressure of the draw solution used in PRO [36]. Due to the high osmotic pressure at solubility, the identified organic draw solutions can be used at applied hydraulic pressures higher than 4.8 MPa to achieve a high peak power density (excluding CaAc, with a peak power density at 3.5 MPa applied hydraulic pressure) in PRO. The currently available commercial membrane can tolerate up to 4.8 MPa applied hydraulic pressure during the PRO process [89] as this commercial membrane gets fractured above 4.8 MPa applied pressure. Thus, available membranes cannot be used during the PRO process for the selected draw solutions at their solubility. If a suitable robust membrane is available for the PRO process in future research, the selected organic draw solutions would work efficiently at their solubility/maximum concentration to generate a high peak power density. One adverse effect of high solubility/maximum concentration, high viscosity of the draw solution is expected, causing an increase in pressure (consuming more pumping energy) and mass transport resistance, potentially causing a lower net power generation from the PRO process. A comparison of the peak power density of the studied draw solutions with other draw solutions is shown in Table 6.

Table 6 Comparisons of the peak power density for different draw solutions in the PRO experiment

Draw solutions			Membrane	Feed	W_{max} (W/m^2)	Ref.
Name	Conc.	Osmotic pressure (MPa)				
$Na_5[Fe(C_6H_4O_7)_2]$/ Water	1 M	-	TFC PRO hollow fiber (Fabricated)	DI water	16.2	[74]
LiCl/Methanol	1 M	~ 6	Commercial TFC, HTI, Albany, OR		8.37	[54]
NaCl/Water	1 M	4.8			~ 10.7	[90]
KCit/Water	0.62 M	2.8			11.10	This report
CaAc/Water	1.22 M				12.03	
KOxa/Water	0.55 M				12.45	
KAc/Water	0.97 M				12.72	
NH_4Ac/Water	1.32 M				13.03	
NH_4C/Water	0.58 M				13.55	
NH_4F/Water	0.91 M				13.69	
KF/Water	0.99 M				13.87	
NaGly/Water	1.07 M				14.36	
NaP/Water	1.01 M				14.59	
CaP/Water	0.87 M				14.64	
NaCl/Water	0.93 M				10.21	
NH_4HCO_3/Water	1.03 M				9.57	

3.8 Compatibility of the organic draw solutions with the commercial TFC membrane

The compatibility of the draw solution with the membrane is an important issue when selecting a draw solution for an osmotic process. If a draw solution reacts with the membrane, performance can decline. For this reason, the compatibility of the selected organic draw solutions with the commercial TFC membrane was tested by investigating the pure water permeability and the salt permeability of the membrane. In a cross-flow RO cell, the pure water and salt permeability of the TFC membrane was investigated before and after conducting PRO experiments by using the organic draw solutions separately. The water permeability of the TFC membrane before conducting the PRO experiments was 32.5 LMH/MPa. The water permeability of the TFC membrane after conducting the PRO experiments with each organic draw solution was consistent, at a value of 32.5 LMH/MPa (Figure 11A). The salt permeability of the TFC membrane before

and after conducting the PRO experiments with each organic draw solution was also consistent, and it is presented in Figure 11 B. These results demonstrated that the commercial TFC membrane is compatible with the selected organic draw solutions.

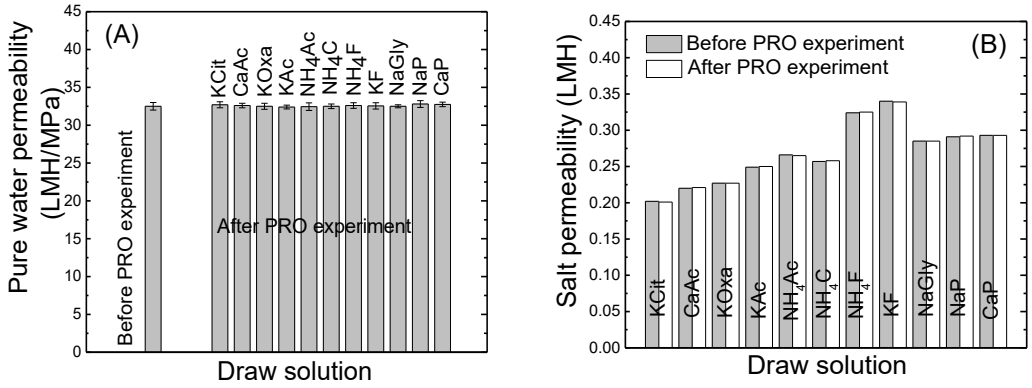

Figure 11 (A) Pure water permeability and (B) salt permeability of the membrane before and after the PRO experiment with each organic draw solution

3.9 Studies on the organic draw solutes for recovery in the downstream of the PRO process

A laboratory investigation using the gravimetric method was conducted to distinguish the organic draw solutes as distillable or thermolytic. Using this method, an amount (W_1) of a draw solute was dissolved in DI water and then the solution was heated to 50 °C to evaporate all the water. The weight (W_2) of the residue was measured again after evaporating all the water from the solution. Finally, the osmotic pressure of the residue (when $W_1 = W_2$) at the same concentration of the draw solute was investigated. The W_1 and W_2 values were consistent for the draw solutes KCit, CaAc, KOxa, KAc, KF, NaGly, NaP and CaP (Table 7). Moreover, the osmotic pressures of the draw solute and the corresponding residue at the same concentration were similar for these draw solutes (Table 7). These results revealed the distillable properties of these draw solutes. The W_1 values were higher than that of W_2 for the draw solutes of NH_4Ac, NH_4C, and NH_4F, which demonstrated the thermolytic properties of these three draw solutes (Table 7). Ammonium acetate decomposed into acetamide (solid) and water under applied heat [91]. Ammonium carbamate decomposed into

ammonia and carbon dioxide gases at 50 °C. Formamide (liquid) and water were produced by the decomposition reaction of ammonium formate under heat [92].

Table 7 A list of the organic draw solutes indicating if they are thermolytic or distillable at 50 °C

Draw solute	Conc. (g/L)	Relation between W_1 and W_2	Osmotic pressure (MPa)		Type
			Pristine	Residue	
KCit	134.81	$W_1 = W_2$	2.80	2.80	Distillable
CaAc	129.70	$W_1 = W_2$	2.80	2.81	Distillable
KOxa	66.00	$W_1 = W_2$	2.80	2.80	Distillable
KAc	64.80	$W_1 = W_2$	2.80	2.80	Distillable
NH_4Ac	70.14	$W_1 > W_2$	2.80	Residue available	Thermolytic
NH_4C	30.04	$W_1 > W_2$	2.80	No residue	Thermolytic
NH_4F	39.30	$W_1 > W_2$	2.80	No residue	Thermolytic
KF	57.20	$W_1 = W_2$	2.80	2.79	Distillable
NaGly	72.05	$W_1 = W_2$	2.80	2.80	Distillable
NaP	66.30	$W_1 = W_2$	2.80	2.79	Distillable
CaP	108.00	$W_1 = W_2$	2.80	2.80	Distillable

The effect of the solute content on the evaporation rate of the solvent (water) from the solution was also investigated for all selected organic draw solutes. The solvent evaporation rates from the organic draw solutions at different initial concentrations are shown in Figure 12. The evaporation rate of DI water at 50 °C is 6.25 mL/h (Figure 12A). The solvent evaporation rates for all the draw solutions at the initial concentration of 0.75 M were almost identical to that of pure water (Figure 12A). However, the solvent evaporation rates from all the draw solutions at a 2 M initial concentration were lower compared to pure water due to the higher interaction between the water molecule and draw solute (Figure 12B). The solvent evaporation rates from the draw solutions were also different at a 2 M initial concentration (Figure 12B). This phenomenon can be explained as the chemical bond between the hydrogen and oxygen atoms in the water molecule is a polar covalent bond. The polar covalent bond in the water molecule forms a hydrogen bond with another hydrogen, and when water is heated, the intermolecular attraction (hydrogen bond) in water is broken down as the water molecules evaporate. The draw solutes are carboxylic acid salts, which are strong electrolytes and ionize completely in water, causing the cations and anions of the organic salts to interact with the polar water molecules. In its aqueous solution, one mole of sodium propionate dissociates into one mole of Na^+ ion and one mole of propionate ion. These Na^+ and

propionate ions interact with the water molecules. To evaporate the water molecules from the sodium propionate solution, three types of interactions, water-water, water-Na^+ ion and water-propionate ion, need to be broken down. Hence, the water evaporation rate from the sodium propionate solution is lower (5.04 mL/h) (Figure 12B) than that of pure water.

Compared to the sodium propionate solution, the water evaporation rate is slightly lower for the NaGly solution due to its additional polar –OH group. The –OH group causes an additional interaction with the water molecule that slows the evaporation rate of water. The interaction of a cation (metallic ion) with the water molecule is dependent on the size of the cation. The smaller sized cations show higher interaction rates with the water molecules due to the lower distance of the water molecule from the nucleus of the metallic ion. The sizes of the Na^+ and Ca^{2+} ions are almost identical as presented in Table 8. One mole of CaAc and CaP contain two moles of anions each that show higher interactions (than that of NaP) with water molecules. Hence, a slightly lower water evaporation rate (4.86 mL/h) was obtained for CaAc and CaP solutions.

Table 8 A list of the organic draw solutions with their molecular formula and ions

Draw solution	Molecular formula	Cation	Anion	Radius of cation
NaP	CH_3CH_2COONa	Na^+	$CH_3CH_2COO^-$	102 pm [93]
NaGly	$HOCH_2COONa$	Na^+	$HOCH_2COO^-$	
CaAc	$(CH_3COO)_2Ca$	Ca^{2+}	$(CH_3COO^-)_2$	100 pm [93]
CaP	$(CH_3CH_2COO)_2Ca$	Ca^{2+}	$(CH_3CH_2COO^-)_2$	
KF	HCOOK	K^+	$HCOO^-$	138 pm [93]
KAc	CH_3COOK	K^+	CH_3COO^-	
KOxa	KOOC-COOK	K^+	$^-OOC\text{-}COO^-$	
KCit	$HOC(COOK)(CH_2COOK)_2$	K^+	$HOC(COO^-)(CH_2COO^-)_2$	
NH_4F	$HCOONH_4$	NH_4^+	$HCOO^-$	-
NH_4Ac	CH_3COONH_4	NH_4^+	CH_3COO^-	
NH_4C	$H_2NCOONH_4$	NH_4^+	H_2NCOO^-	

The size of the K^+ ion is greater than that of the Na^+ and Ca^{2+} ions (Table 8). For this reason, the K^+ ion shows lower interaction with water molecules than that of the Na^+ and Ca^{2+} ions. The lower attraction of K^+ ion to water molecules demonstrated the higher solvent evaporation rate from the KF and KAc solutions. However, the solvent evaporation rate was lower for the KOxa and KCit

solutions due to the presence of two K^+ ions and two negative charges on the oxalate ion in a KOxa molecule and three K^+ ions, three negative charges, and one polar –OH group from the citrate ions in a KCit molecule.

The NH_4^+ ion is a nonmetallic ion that shows relatively lower attraction to water molecules. Hence, the solvent evaporation rate from the NH_4F, NH_4Ac and NH_4C solutions was higher than that of other solutions. In addition, these three draw solutes are thermolytic, decomposing to produce gaseous products under heat. The gaseous products obtained from the decomposition of these three draw solutions accelerate the evaporation of the water molecules.

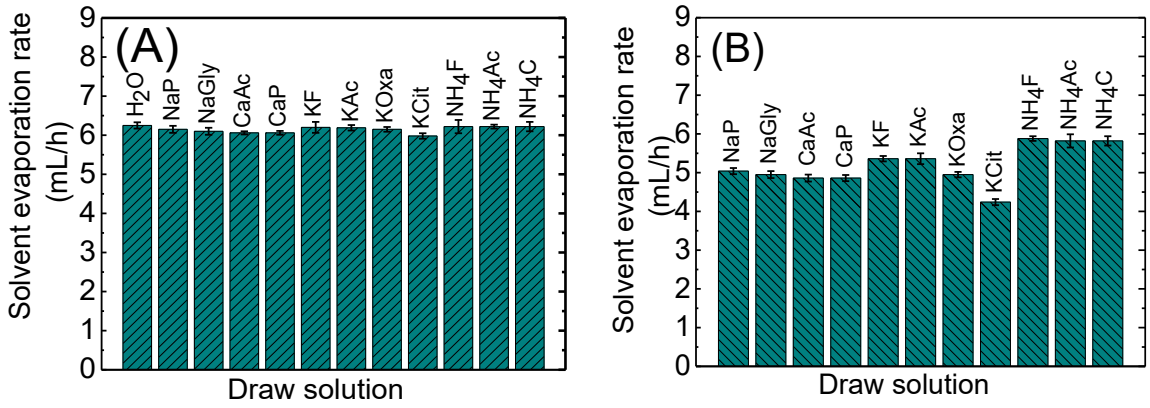

Figure 12 Solvent evaporation rate from the organic draw solutions at 50 °C and an initial concentration of (A) 0.75M and (B) 2M

Based on the results, the distillable draw solutes can be recovered from the solution by using the membrane distillation technique in downstream of the PRO process. Membrane distillation is an emerging technology that utilizes low-grade heat or industrial waste heat with a temperature of ~50 °C to drive the separation of the solute from a solution [94]. The existing pilot-scale, membrane-based osmotic process uses industrial waste heat to recover the draw solutions during the downstream separation of osmotic processes [73,95]. Ammonium carbamate (thermolytic) can be separated from its solution by using thermal distillation at a low temperature (~50 °C) downstream of the PRO process. This draw solute decomposed into ammonia and carbon dioxide gases at 50 °C, which could be regenerated by the reaction between the resulting ammonia and

carbon dioxide gases [96]. This type of recovery and regeneration method during the osmotic process is currently being used for the NH_4HCO_3 draw solute (thermolytic) [72].

3.9 Suitable organic draw solutions for the closed-loop PRO application

Peak power density and recyclability are two significant parameters for gauging the effectiveness of the selected organic draw solutions in the closed-loop PRO process. The draw solutions that can produce a high peak power density, can be easily separable and recyclable are desirable for application to the closed-loop PRO. The order of peak power density (W/m^2) for the organic draw solutions at 4.2 MPa osmotic pressure is CaP (14.64)> NaP (14.59)> NaGly (14.36)> KF (13.87)> NH_4F (13.69)> NH_4C (13.55)> NH_4Ac (13.03)> KAc (12.72)> KOxa (12.45)> CaAc (12.03)> KCit (11.10). As discussed in the previous section, all the distillable organic draw solutions can be separated and recycled using a membrane distillation technique. Amongst the thermolytic draw solutions, only NH_4C can be separated by thermal distillation process followed by regeneration (for reuse in the closed-loop PRO) from the decomposable products of this draw solution. The order of potentiality for the organic draw solution application in a closed-loop PRO coupled with membrane distillation as downstream separator: CaP (14.64) > NaP (14.59)> NaGly (14.36)> KF (13.87)> KAc (12.72)> KOxa (12.45)> CaAc (12.03)> KCit (11.10). NH_4C holds the greatest potential among the organic draw solutes for applications to the closed-loop PRO when thermal distillation is used as a downstream separator.

3.10 Non-fouling propensity of the organic draw solutions in the PRO process membrane

Not all organic compounds are responsible for the organic fouling of the membrane used in the PRO process. Usually, the organic matter consists of humic substances, polysaccharides, proteins, lipids, nucleic and amino acids, organic acids and alcohols can cause the organic fouling of the membranes used in the osmotic process [97]. These organic matters are not completely dissociable into water. In our study, all the draw solutions were organic salts that completely ionized in water. Thus, it can be said that the organic draw solutions studied in this research could not cause the organic fouling of the membrane used in the PRO process.

Another type of membrane fouling that can occur during the PRO process is scaling. Scaling is due to the formation of $CaSO_4$ and $CaCO_3$ on the membrane surface [98,99].These two salts ($CaSO_4$ and $CaCO_3$) are partially soluble in water, which is why they are responsible for the scaling of the membrane during the osmotic process. However, the identified organic draw solutions in this study are highly soluble in water. For this reason, the identified organic draw solutions would not cause any membrane fouling through scaling during the PRO process.

3.11 Potential of renewable power generation by closed-loop PRO

In this research, it is proposed that hydrostatic energy obtained from closed-loop pressure retarded osmosis using the identified organic draw solutions can be converted into electrical energy by utilizing a water turbine. Currently used water turbine can demonstrate up to 90% efficiency [100-101]. Therefore, it can be assumed that up to 90% of sustainable energy could be generated by using the proposed closed-loop pressure retarded osmosis process reported in this paper.

3.12 Conclusions

A successful database-driven screening method was used to select potentially effective organic draw solutions for applications to the PRO process. The performance of the selected organic draw solutions was evaluated using a commercial TFC membrane in the PRO process. During this process, the organic draw solutions (excluding KCit) demonstrated 1.06% to 18.69% and 6.9% to 25.56% higher peak power densities compared to NaCl and NH_4HCO_3, respectively, at 2.8 MPa osmotic pressure. At this osmotic pressure, the KCit draw solution demonstrated 6.17% and 0.75% lower peak power density compared to NaCl and NH_4HCO_3, respectively. However, 8.72% to 43.39% and 15.99% to 52.98% higher peak power densities were obtained for the organic draw solutions at 4.2 MPa osmotic pressure. The 2.09 to 2.18-times increase in peak power density for the organic draw solutions, as well as 1.8 times for NaCl and 1.79 times for NH_4HCO_3 were achieved when increasing from 2.8 MPa to 4.2 MPa osmotic pressure in the PRO experiments. This trend indicates that the organic draw solutions can generate much higher peak power densities than those of NaCl and NH_4HCO_3 at osmotic pressures higher than 4.2 MPa. The selected organic draw solutions were also tested for a potential recovery method in the downstream of the PRO

process. The laboratory investigation revealed that the membrane distillation and thermal distillation (at ~50 °C) techniques are potential recovery methods for the selected draw solutions (excluding NH_4Ac and NH_4F). The high peak power density and potential recovery methods could make the selected organic draw solutions commercially viable for applications to the closed-loop PRO process.

In this research, theoretical peak power density, calculated by experimental water flux and applied hydraulic pressure values in PRO, has been reported for the identified organic draw solutions. Real peak power density in PRO for these draw solutions could be investigated in the future research by further increasing osmotic pressures. Membrane distillation and low temperature thermal distillation are proposed as potential downstream separation methods to recycle the draw solutions in PRO in this research. In future research, the identified draw solutions could be used in the combined process composed of PRO and membrane distillation/low thermal distillation to investigate the real performance of these draw solutions.

Chapter 4: Effect of temperature on closed-loop PRO with potential organic draw solution

4.1 Introduction

Global energy demand rose by 2.1% in 2017, more than twice compared to 2016's rate, boosted by global economic growth, with oil, gas, and coal monopolizing most of the increase in demand for energy, with renewables seeing impressive gains as well [102]. Unfortunately, the extensive use of fossil fuels (oil, gas, coal) has a major role in environmental pollution and climate change. Recent study reported that global warming is mainly caused by CO_2 emissions from fossil fuels [103]. To mitigate these effects, The International Renewable Energy Agency (IRENA) claimed that renewable energies are the key climate solution [104]. Pressure retarded osmosis (PRO) is a membrane-based technology that produces green energy by converting the osmotic pressure difference between two solutions with different salinities to electricity, without producing CO_2 [1,42]. It has been estimated that global osmotic power potential is equivalent to around 2.6 TW/year, which could be even higher if Reverse Osmosis (RO) brine from RO desalination facilities is taken into consideration [70,105]. Intermittent renewable energy sources (solar, wind turbines, etc.) cannot provide a continuous supply of energy. Therefore, to get energy without interruption, PRO is a potentially viable alternative technology. The threshold of achieving a power density greater than 5 W/m^2 has been discussed as a requirement for the economic viability of PRO [68]. To make it viable, several investigations were carried out to optimize the energy production by; high permeability PRO membranes fabrication [106–109], PRO process design studies [110–113], detrimental effects mitigation [114–116] and operating conditions optimization [117]. Two types of PRO design were proposed and investigated, namely closed-loop PRO and open-loop PRO. Closed-loop process was considered more advantageous in terms of performance, efficiency and environmental consideration. This is because there is no limitations regarding draw solutions, the capacity of regenerating draw and feed solutions, capability of smooth operation at any convenient places and environmental friendly features. Generally, closed-loop PRO is composed of three main parts, namely the PRO unit for the utilization of osmotic pressure difference between different salinity gradient solution, water turbine for generation of power and downstream separation process. The effect of operating temperature can play a significant role in overall power production in PRO process since it affects solution physicochemical properties like

viscosity, density, and diffusion [118] as well as membrane hydrodynamic properties [119], proven through previous investigations [2, 118–121]. This increasing of temperature in a closed-loop PRO process through the utilization of low-grade waste heat is a growing concern. The exact quantity of industrial waste heat is poorly quantified, but various studies have estimated that as much as 20 to 50% of industrial energy consumption is ultimately discharged as waste heat [57]. [4]. During the closed-loop PRO process, thermal and membrane distillation processes can be used to regenerate thermolytic and distillable draw solutes, respectively, using industrial waste heat. Thanks to these results, the concept of utilizing low-grade waste heat in closed-loop PRO seems to be very promising for the sustainability of the total system. Installment of closed-loop PRO system within the close proximity of power plants, solar panels, breweries, etc. where a large amount of energy is being lost as waste heat can make this process more feasible [54]. However, these previous studies were focusing on the temperature effects for simulated seawater or RO brine solutions. In other words, the solute used was purely inorganic. Experiments showed that even if the power density increased, operational limitations such as membrane deformation or deterioration and intense fouling can be expected with a severe salt leakage. No completed works have been performed to investigate the performance of PRO using organic solutes under elevated operating temperature. In this research, closed-loop PRO with membrane distillation (MD) as solution regeneration system was used to investigate the effect of temperature on the water flux, power density and reverse solute flux. Experiments were carried out using a commercial TFC FO flat sheet membrane to understand the temperature-induced interaction between solute, water, and membrane. Organic (sodium propionate and potassium acetate) and inorganic (NaCl) draw solutions were used for comparison. The organic solutes were carefully selected based on physical state at ambient temperature and pressure, toxicity, solubility, and osmotic pressure. Suggested draw solutions were first tested with deionized water as feed solution. First, membrane transport properties and parameters were determined under PRO mode (active surface facing towards draw solution) for all studied solutions. Then, draw solutions were tested under different operating temperatures. The range of temperatures selected is from 20°C to 40°C to simulate heat waste utilization. Analysis and comparison of experiments result in term of water flux, power density and salt diffusion were performed. Finally, implication on large-scale PRO process was enumerated for better the understanding of crucial parameters that should be optimized for maximum energy production.

4.2 Theoretical background

4.2.1 Water and salt fluxes

Water permeation flux, J_w, across a semi-permeable membrane that allows water passage but rejects solute molecules or ions. This is related to the water permeability, A, the effective osmotic pressure difference, $\Delta\pi_m$, and the transmembrane hydraulic pressure difference, ΔP, as follows [36]:

$$J_w = A\,(\Delta\pi_m - \Delta P) \quad \text{.....(15)}$$

$$\Delta\pi_m = \pi_{D,m} - \pi_{F,m} \quad \text{.....(16)}$$

where $\pi_{D,m}$ and $\pi_{F,m}$ are the osmotic pressure at the surface of the active and support layers respectively. ΔP is the applied hydraulic pressure. Similarly, the reversal salt flux can be expressed as [36]:

$$J_s = B\,(C_{D,m} - C_{F,m}) \quad \text{.....(17)}$$

where B is the salt permeability coefficient, $C_{D,m}$ is the concentration at the active layer facing draw solution, and $C_{F,m}$ corresponds to the concentration at the interface of the active layer facing feed solutions. In osmotically driven processes, concentration polarization (CP) plays a very influential role by reducing the water flux [122,123]. The governing water flux equation for the PRO process should incorporate the effect of CP. When using non-ideal membranes, dilutive External Concentration Polarization ($ECP_{dilutive}$) occurs when the feed solution permeates through the active layer and enters into the draw side and dilutes the salt concentration, $C_{D,m}$, and lowers the osmotic pressure difference. Due to the $ECP_{dilutive}$, driving force decreases and water flux reduces. Mathematically, $ECP_{dilutive}$ can be expressed as:

$$\frac{\pi_{D,m}}{\pi_{D,b}} = \exp\left(-\frac{J_w}{k}\right) \quad \text{.....(18)}$$

Where k is the mass transfer coefficient which is calculated using the following formula:

$$k = \frac{ShD}{d_h} \quad \text{.....(19)}$$

Here, d_h is the hydraulic diameter and *Sh* is the Sherwood number for the appropriate flow regime in a rectangular channel, which is be defined as [36] :

$Sh = 1.85\ R_e S_c\ \frac{d_h}{L}$ (if laminar flow)……...……(20)

$Sh = 0.04\ {R_e}^{0.75} {S_c}^{0.33}$(if turbulent flow)……..……..……(21)

where R_e is the Reynolds number, S_c the Schmidt number and L is the length of the channel.

$S_c = \frac{\mu}{\rho D}$ ……..……..……..…(22)

$R_e = \frac{vd\rho}{\eta} = \frac{vd}{\mu}$ ……..……..……..…(23)

D in the above equation denotes diffusivity, μ is kinematic viscosity, v is the dynamic viscosity and v is the velocity of the flow. In PRO mode (the active layer facing the draw solution), Internal Concentration Polarization (ICP) occurs when the low concentrated solution flows through the porous support layer and eventually passes cross the active layer. Simultaneously, the reverse salt flux, J_s, permeates salt in the opposite direction of J_w. This leads to a salt gradient in the membrane support layer. ICP can be expressed mathematically as follows [123]:

$\frac{\pi_{F,m}}{\pi_{F,b}} = \exp\left(J_w \frac{s}{D}\right)$……..……..…(24)

Assuming one type of solute in the system and the concentration of solutes is proportional to the osmotic pressure, the van't Hoff equation gives:

$\pi = iCRT$ ……..……..…(25)

where β is the van't Hoff coefficient (i = 2 for NaCl), R is the gas constant and T is the absolute temperature. Taken into account ECP, ICP and J_s, the draw concentration at the active layer surface ($C_{D,m}$), the feed concentration at the active layer surface ($C_{F,m}$), the water flux, J_w, and the salt flux, Js, are expressed as follows [27]:

$C_{D,m} = C_{D,b} \exp\left(-\frac{J_w}{k}\right) - \frac{B}{J_w}\left(C_{D,m} - C_{F,m}\right)\left[1 - \exp\left(\frac{-J_w}{k}\right)\right]$……..……..(26)

$C_{D,m} = C_{F,b} \exp\left(\frac{J_w}{D} s\right) + \frac{B}{J_w}\left(C_{D,m} - C_{F,m}\right)\left[\exp\left(\frac{J_w}{D} s\right) - 1\right]$……..…..(27)

$J_w = A\left(\frac{\pi_{D,b} \exp\left(\frac{-J_w}{k}\right) - \pi_{F,b} \exp\left(J_w \frac{s}{D}\right)}{1 + \frac{B}{J_w}\left[\exp\left(\left(J_w \frac{s}{D}\right) - exp\left(\frac{-J_w}{k}\right)\right)\right]} - \Delta P\right)$……(28)

$$J_s = B\left(\frac{C_{D,b}\exp\left(\frac{-J_W S}{D}\right)-C_{F,b}\exp\left(\frac{J_W}{k}\right)}{1+\frac{B}{J_W}\left[\exp\left(\left(\frac{J_W}{k}\right)-exp\left(\frac{-J_W S}{D}\right)\right)\right]}\right) \quad (29)$$

Membrane structural parameters are considered to be constant in some published literature (s= τt/ε) [37,55,119–121]. However, the structural parameter can change with the different operating conditions. These parameters can include pressure and temperature [2-3,118]. The s value was calculated from Eq. (28) as a fitted parameter using selective layer properties (A and B) obtained from RO experiments and the water flux (J_w) conditions of the osmotic flux tests suggested by Manickam and McCutcheon [125]. The PRO power density is then calculated per unit area of the membrane by multiplying water flux and applied hydraulic pressure using Eq.(30):

$$W = J_w \Delta P \quad (30)$$

4.3 Materials and Methods

4.3.1 Closed-loop PRO

Figure 13 describes the studied closed-loop PRO. The draw and feed solution are firstly recirculated to PRO. After exiting the PRO module, the diluted draw solution is used to produce energy via a hydroturbine. Both concentrated feed and diluted draw streams are then conducted to the seperator (membrane distillation) to regenerate the initial feed and draw solutions. The draw stream is always pressurized before entering the PRO module. The applied pressure was chosen depending on the operating conditions and targeted study. As the effect of the temperature is studied here, thermostatic baths were incorporated into the system to control the solutions temperature.

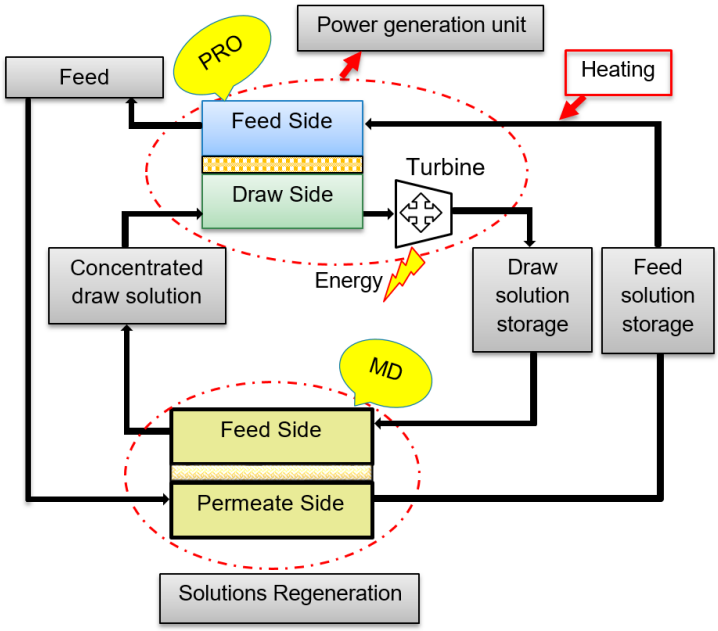

Figure 13 Schematic diagram of closed-loop PRO process

4.3.2 Membrane and chemicals

The commercial thin film composite (TFC) FO membrane used in this study was provided by Porifera (Hayward, CA). The membrane is mechanically supported by an integrated woven mesh support layer. Water was provided by an Integral 10 water system (Millipore Corporation, Billerica, MA). ACS grade sodium chloride, potassium acetate and sodium propionate (provided by Fisher Scientific) were used in this experiment. The ultrapure water with a resistivity of 18.2 MΩ cm was supplied by a Milli-Q system (Millipore Integral 10 water Purification System). The physiochemical parameters (e.g., osmotic pressure and diffusivities) of the sodium chloride, potassium acetate, and sodium propionate solutions were calculated using OLI Stream Analyzer 3.1 (OLI Systems, Inc.). The properties of the membranes will be determined by using conventional method [4]. The membrane has been supported by fabric spacer on the support side. Prior to use, they were soaked in ultrapure water for at least 24 hours. The OLI stream analyzer^{TM} (OLI Systems, Inc.) was used to measure the solution properties such as diffusivity, viscosity and the densities of the sodium chloride, potassium acetate, and sodium propionate solutions. This data is presented in Table 9 and Table 10.

4.3.3 Determination of water permeability, solute permeability coefficients, and membrane structural parameter

Intrinsic water permeability coefficient (A), the salt rejection rate (R) and the salt permeability coefficient (B) was measured for the TFC FO membrane (Porifera, Hayward, CA) using cross-flow RO experiment at three different temperatures, namely 20^0C, 30^0C, and 40^0C. The temperature was well controlled by heated water bathtub. A coupon of the membrane with an effective surface area of 19.94 cm^2 was placed in a stainless steel test cell with active layer against feed stream. A high-pressure hydra-cell pump has been used for the desired pressure into the system as well as for the recirculation of the feed stream. The flow was maintained at 0.5 LPM throughout the experiment. To investigate water permeability coefficient A, three different pressure was applied starting from 50 psi (0.345 MPa) to 150 psi (1.034 MPa) with an increment of 50 psi (0.345 MPa) . De-ionized water was used as feed. For each temperature, the experiment was conducted for 12 hours. The water flux through the membrane was obtained from a liquid flow sensor (Sensirion, The Sensor Company) that was directly connected to a computer. The value of A was determined experimentally using the following formula [2]:

$$A = \frac{J}{\Delta P} \quad \text{.....(31)}$$

Where,

$$J = \frac{\Delta V}{A_m \Delta t} \quad \text{.....(32)}$$

In the above equation, J is the pure water flux, A_m is the effective membrane area, ΔV is the permeate volume, Δt is time and ΔP is the hydraulic pressure difference across the membrane. The salt permeability coefficient (B) was also calculated for the three salts; NaCl, KAc and NaP. The concentration used for each salt was 35 mM and the pressure was maintained constant at 145 psi (1.0 MPa). The salt concentration of the permeate solution was investigated using a calibrated conductivity meter (Oakton, Eutech Instruments). The following equation has been used for the calculation of the salt rejection R_s and B [36]:

$$R_s(\%) = \frac{C_f - C_p}{C_f} \times 100 \quad \text{.....(33)}$$

$$B = \frac{A(1-R)(\Delta P - \Delta \pi)}{R} \quad \text{.....(34)}$$

Here, C_f is the salt concentration of the feed solution, C_p is the salt concentration of the permeate solution and $\Delta\pi$ is the osmotic pressure of the feed solution. To investigate the reverse salt flux, a sample of the feed solution was collected before and after the experiment to determine the salt concentration using a calibrated conductivity meter (Oakton, Eutech Instruments). The reverse salt flux was determined experimentally using the following equation [2]:

$$J_s = \frac{C_f V_f - C_{f,i} V_{f,i}}{A_m \Delta t} \quad \text{.....(35)}$$

where C_f and V_f are the salt concentration and total volume of the feed at the end of the tests, respectively, and $C_{f,i}$ and $V_{f,i}$ are the initial salt concentration and total volume of the feed, respectively. A_m is the effective membrane surface.

4.3.4 PRO experiments

A lab-scale PRO system (presented in Figure 14) was used to measure the water flux and reversal salt flux under true PRO conditions in the coupon cell. Inorganic salt sodium chloride, organic salt potassium acetate, and organic salt sodium propionate were used as draw solution. All the experiments were conducted for 1M draw solution. Distilled water was used for feed solution throughout the experiments. This PRO performance study was conducted for three different feed solution temperatures 20^0C, 30^0C and 40^0C while draw solution temperature was maintained at 20^0C. The temperature of both feed and draw solution was controlled using a recirculating chiller/ heater (PolyScience, IL, USA). The thermometer was used to determine the temperature of the solutions. Draw, feed and draw bypass flow was recirculated through a custom membrane cell with channel dimensions of 7.5×4×0.25 cm. Feed channel was supported by pre-wet woven fabric to provide enough protection against membrane deformation due to the pressurized draw solution. An EPDM O-ring was used in the draw side to prevent any possible leakage during the experiment. 4 L reservoir was used for both the feed and draw solution. A hydra-cell, the high-pressure pump, was used to circulate the draw solution at specific velocities (flow rate for both draw and feed solution was 0.5 L/min). Containers for each of the feed and draw solutions were placed on analytical balances (Sartorius Corporation, Bohemia, NY) to provide weight and water flux has been measured gravimetrically.

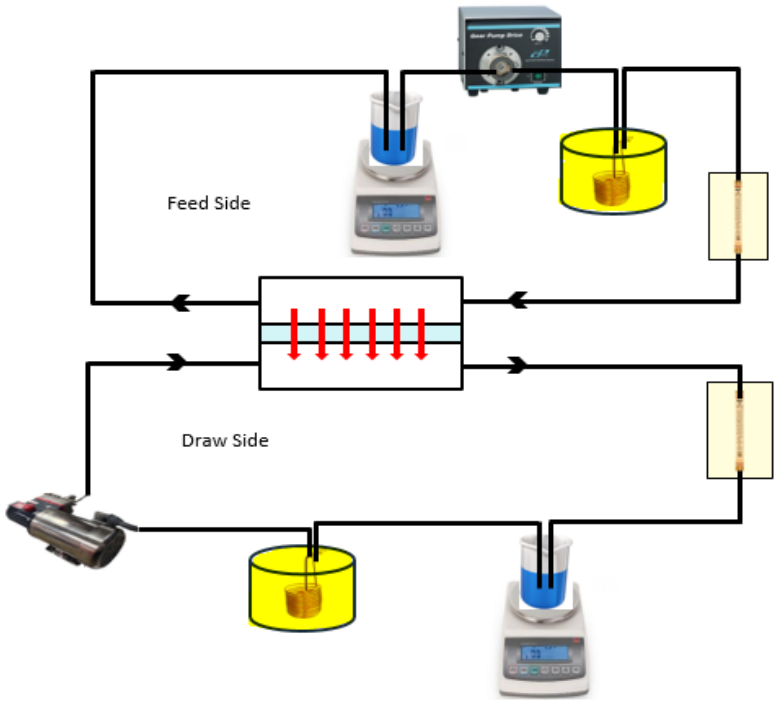

Figure 14 Lab-scale PRO set up

A calibrated conductivity meter was used to measure the conductivity of the feed solution. Pristine membrane samples were tested in each trial with actual PRO condition i.e. an active layer of the membrane facing draw solution. Conductivity was evaluated at three different feed solution temperatures: 20^0C, 30^0C and 40^0C. At each of these temperatures, the three draw solutions, namely NaCl, KAc and NaP, were tested with 1M concentrations. The pressure was increased from 0 psi (0 MPa) to 100 psi (o.689 MPa) with an increment of 25 psi (0.172 MPa) for each trial. At each pressure, PRO testing was completed for 30 minutes to get the stable data.

4.4 Results and Discussions

4.4.1 Membrane transport properties

The water permeability coefficient is very important for determining the performance of the membrane, whereas the salt permeability coefficient plays a significant role in the PRO process as it acts as an influential parameter for the performance of the process [126]. Table 9 presents the

Table 9 Summary of the membrane and draw solution properties for 1 M draw solutions

Draw Solutions	Temperatures	Separation parameters			Diffusivity D (m^2/sec)× 10^{-9}
		Water permeability (A) (LMH/bar)	Salt permeability (B) (LMH)	Structure parameter (s) μm (Eq. 28)	
NaCl	$T_F = 20^0C$; $T_D = 20^0C$	4.9	2.11	122	1.41
	$T_F = 30^0C$; $T_D = 20^0C$	5.9	3.56	136	2.02
	$T_F = 40^0C$; $T_D = 20^0C$	7.8	5.44	143	2.48
KAc	$T_F = 20^0C$; $T_D = 20^0C$	4.9	0.30	139	2.02
	$T_F = 30^0C$; $T_D = 20^0C$	5.9	0.47	139	2.20
	$T_F = 40^0C$; $T_D = 20^0C$	7.8	0.68	149	2.78
NaP	$T_F = 20^0C$; $T_D = 20^0C$	4.9	0.35	141	1.95
	$T_F = 30^0C$; $T_D = 20^0C$	5.9	0.48	145	2.15
	$T_F = 40^0C$; $T_D = 20^0C$	7.8	0.69	151	2.68

Table 10 Parameters used for modeling

Parameter	NaCl			KAc			NaP		
	20^0C	30^0C	40^0C	20^0C	30^0C	40^0C	20^0C	30^0C	40^0C
k (10^{-7} ms^{-1})	1.155	1.484	1.736	1.450	1.581	1.886	1.384	1.484	1.778
d_h ($\times 10^{-3}$m)	8.573	8.573	8.573	8.573	8.573	8.573	8.573	8.573	8.573
μ ($\times 10^{-3}$ $N.s/m^{-2}$)	1.13	1.096	1.038	1.169	1.0834	1.058	1.226	1.208	1.109
ρ ($\times 10^3$ Kg/m^3)	1.038	1.032	1.024	1.037	1.034	1.026	1.046	1.039	1.030

separation properties (A and B) and the structure parameter (s) of the TFC FO membrane for three different salt (inorganic salt NaCl and organic salt KAc and NaP) at 20^0C, 30^0C, and 40^0C. As temperatures increases, water permeability increases. In fact, similar values of A were observed regardless of the type of the draw solution used, showing that the permeability was not affected by dissolved solutes. Due to the intrinsic tradeoff between permeability and selectivity, B also

increases as the operating temperature was increased. Unfortunately, this leads to an increase of the reverse solute diffusion and the accumulation of the solute within the membrane support layer and in the bulk feed solution. Reverse solute diffusion and solute accumulation will adversely impact the PRO performance due to the enhanced ICP and decrease of the osmotic pressure difference [115]. Among the three salts, NaCl shows the maximum B value compared to other organic salts KAc and NaP, which means NaCl has the lowest retention for TFC FO membrane. Values of s were calculated using Eq.(28) as a fitted parameter. These values should reduce experimentally because of the pressure and temperature effects the membrane, as mentioned in previous works [2,118]. Since Eq. (28) does not take into consideration these effects, s calculation showed to be increasing. Consequently, for more accuracy, the experimental values of s were used in modeling and simulations.

4.4.2 Effect of operating temperatures on PRO performance

4.4.2.1 Effect on water flux

In this section, the effect of temperature on water flux and power density was investigated for three different draw solutions. Figure 15 shows the variation of the water flux power density as a function of applied pressure ΔP for a 1 M draw solution concentration. Experiments were conducted for three different feed solution temperatures (20^0C, 30^0C and 40^0C) while draw solution temperature was kept constant (i.e. 20^0C). Obviously, at fixed temperature, increasing hydraulic pressure leads to the increase of power density. For the three solutions studied, the increase of the temperature is followed by the increase of the water flux and, hence, the power density. In fact, for NaCl, the power density increased by about ~34% (6.7 Wm^{-2} to 9.0 Wm^{-2}) when the temperature was increased from 20^0C to 40^0C. For organic salts, it has been found that potassium acetate shows ~31% (8.5 Wm^{-2} to 11.1 Wm^{-2}) and sodium propionate shows ~27.2% (8.1 Wm^{-2} to 10.3 Wm^{-2}) increase of power density while increasing the operating temperature in the same range of temperature. Similar results were observed for the NaCl draw solution in a previous study [2,120]. These results can be attributed to the fact that increasing the temperature increases the water diffusivity across the membrane, which enhances the performance of PRO. In addition, temperature elevation enhances the hydrodynamics of the process. The thickness of the membrane boundary layer reduces with the temperature increase which leads to the increase of the mass transfer coefficient [118]. Consequently, the ECP is reduced. Moreover, Table 10 shows that

the viscosity of the draw solutions decreases with temperature, especially for the case of potassium propionate. As a result, the mass transfer is enhanced, and the concentration polarization is reduced. Overall, the increase of operating temperature improves the water permeability, reduces CP due to enhanced mass transfer, improves hydrodynamics, decreases the fluid viscosity and increases its diffusivity across the membrane, which leads to markedly improved performance of the process. Thermodynamically, recent work showed that the maximum energy extractable by PRO is directly proportional to the operating temperature [127]. The organic draw solutions showed better performance in term of energy production compared to NaCl, as explain in 4.5.

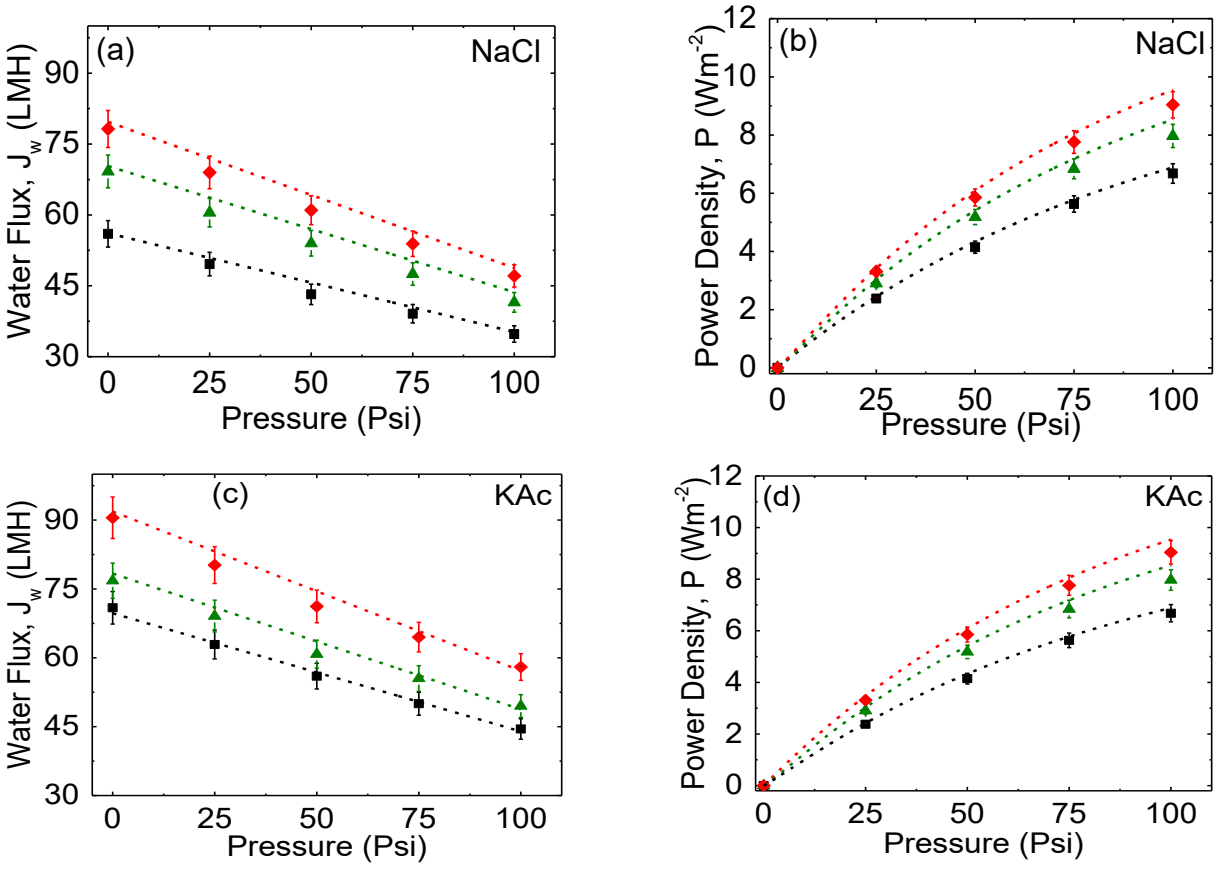

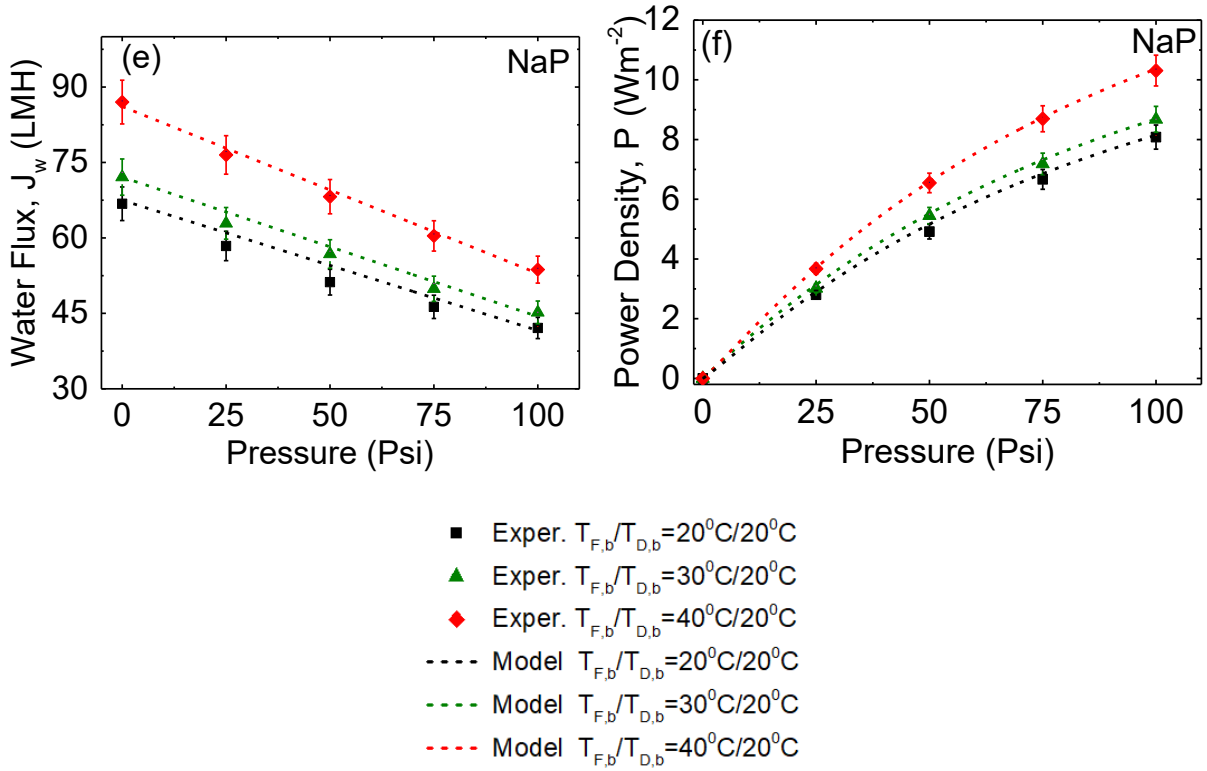

Figure 15 Experimental and modeled water flux & power density of the TFC FO membrane as a function of draw solution pressure for three different draw solutions a & b) NaCl; c & d) KAc; e & f) NaP for different working temperatures T_F=20°C/T_D=20°C, T_F=30°C/T_D=20°C and T_F=40°C/T_D=20°C; Draw flow velocity was 0.5 liters/min, Feed flow velocity was 0.5 liters/min

4.4.2.2 Effect on reverse salt flux

This section discusses the effect of temperature on reverse solute diffusion as well as the specific solute flux. For that, these two parameters were assessed as a function of working temperature and applied pressure. Figure 16 shows that the increase of the temperature causes the increase of both salt flux and specific solute flux regardless of the type of solute. This is due to the tradeoff between water permeability and salt diffusion. In fact, as pressure increases, the solutes in the draw solution gain more energy to surpass the active layer. It is hypothesized that the tensile stress developed in the membrane may stretch the polymer chains in the rejection layer and enlarge the membrane pores to cause a reduced solute rejection [7,79]. It was also shown that, for polymeric membrane, the water permeability and the salt permeability are empirically related by $B = \gamma A^3$ where γ is a fitting parameter [124]. It is clearly shown that the cubic dependence of salt permeability on the water permeability indicates that increases to the water permeability leads to high salt diffusion

and reduce the membrane selectivity. However, this correlation was developed for simulated seawater (NaCl) and cannot be applied for organic solute due to the difference on molecules size, hydration and, diffusivity. Both experimental and numerical analysis shows a good correlation between water flux, reversal salt flux, and power density. Unlike RO testing where the membrane is well supported by a permeate collector, a typical coarse feed spacer may not be sufficient to support the membrane in PRO tests. Furthermore, the deformation of the membrane under pressure can potentially block the feed solution channel, thus increasing pumping energy requirement for feed solution recirculation. It is shown that NaCl salt has not only higher reversal salt flux, but also it shows very high specific solute flux compared to organic salts. Moreover, inorganic salt NaCl exhibits a significantly higher value compared to organic salt KAc and NaP. For example, at an applied pressure of 100 psi (0.689 MPa), J_s value for NaCl shows to be more than 5 times higher value compared to both organic salts when the feed solution temperature is 20^0C. For higher temperature, organic salt diffusion is almost 84.5% less than the NaCl diffusion at 40^0C under 100

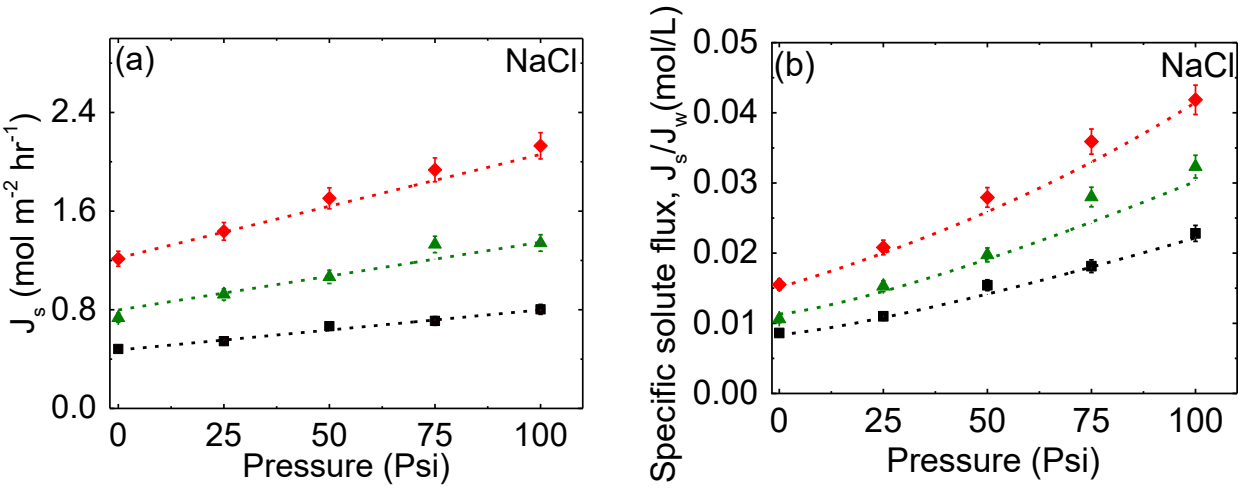

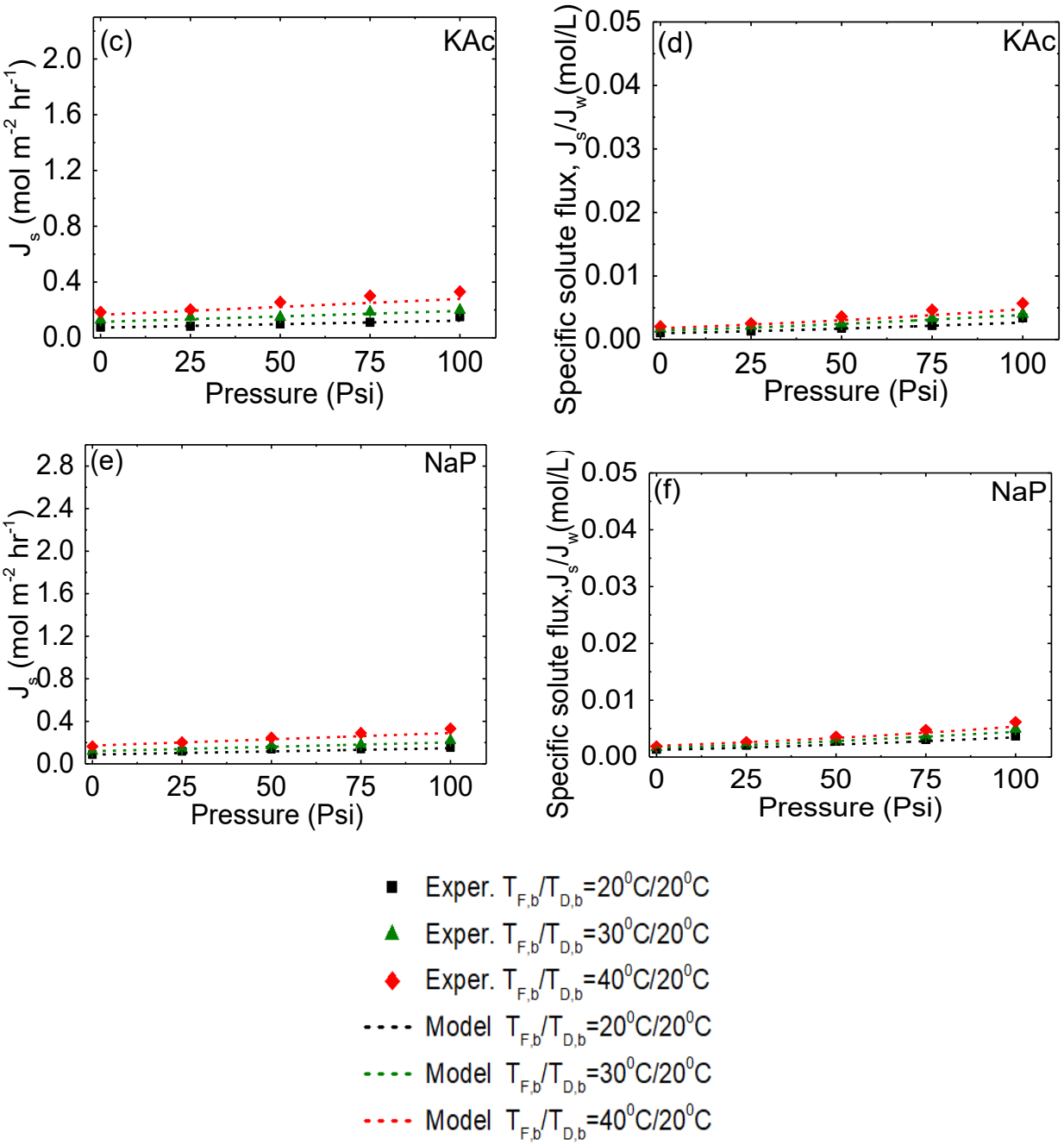

Figure 16 Experimental and modeled reversal salt flux (Js) and specific solute flux (Js/Jw) of the TFC FO membrane as a function of draw solution pressure for three different draw solutions a & b) NaCl; c & d) KAc; e & f) NaP for different working temperatures T_F=20^{0}C/T_D=20^{0}C, T_F=30^{0}C/T_D=20^{0}C and T_F=40^{0}C/T_D=20^{0}C; Draw and feed flow velocity were 0.5 liters/min

psi (0.689 MPa), which confirms that the tradeoff correlation between A and B mentioned previously is not valid for organic solutes. More importantly, the change in temperature is not prominent for reversal salt flux for KAc and NaP, which justifies the potential of these organic salt as PRO draw solution. This behavior is attributed to the significantly lower value of the solute permeability coefficient B for organic salts. (see Table 9). Also, anions in KAc and NaP draw solutions contains larger hydrated ions with the C-O double bond. Due to having a lone pair of electrons in C-O double bond (π-bond), there could be a possible polarization. This polarization effect can be surrounded by many water molecules, forming bigger sizes of the hydrated anions which will eventually prevent ions to pass through the membrane. Furthermore, the propionate and acetate ions contain bulky ethyl ($-C_2H_5$) and methyl ($-CH_3$) groups, respectively. Potassium acetate and sodium propionate also have less permeability across the membrane compared to NaCl. This will result in significantly lower reversal salt flux. Higher mutual diffusivity could be another reason for getting lower reversal salt flux. If any salt has higher diffusivity, this means the solute will diffuse from higher concentration to lower concentration. As dilutive ECP occurs due to the freshwater flow from feed solution to draw solution, it may lower the concentration at the surface of the membrane active layer. This induces a reduction of the effective osmotic pressure between the two sides of the membrane. Since the organic draw solution has higher diffusivity, it contributes to minimize the effect of the dilutive ECP.

4.5 Implication on power production

Herein, a comparative study of power generation using different draw solutions at different operating temperatures was carried out. Figure 17 shows the study of power generation of KAc and NaP w.r.t NaCl. As it can be seen from Figure 17, for all investigated cases, power generation increases with the increase of temperature. When feed solution temperature is raised up to 40^0C, KAc draw solution is associated with 23.2% increase of power while sodium propionate draw solution shows 14.1% higher power generation when compared to NaCl draw solution under an applied hydraulic pressure of 100 psi (0.689 MPa). As described previously, KAc and NaP show much lower reversal salt flux. During the experimental process, due to the lower J_s, there will be a very minimum impact of concentration polarization when compared with NaCl. As concentration polarization can potentially reduce the effective driving force by lowering the osmotic pressure difference between two sides of the membrane, the organic salt shows higher performance in terms

of water flux and power production (since water flux is proportional to the power generation). Besides, higher diffusivity (Table 9) for organic salt shows that it can lower the effect of external concentration polarization (which is dominating when DI water is being used as feed solution). However, when comparing KAc and NaP draw solutions, it is revealed that KAc shows higher performance than NaP. This can be attributed to the higher osmotic pressure of potassium acetate than sodium propionate as described in Table 11. Hence, the driving force for the former (KAc) organic draw solution is higher than the later one (NaP). Overall, organic salts showed superior performance in term of power generation compared to inorganic salt. Moreover, salt diffusion impact is not only limited to reducing power production. In fact, the accumulation of the salt on the surface of the membrane may cause membrane deformation and/or deterioration. For a large scale-PRO, this will cause increases in capital cost due to the need for membrane changing or cleaning. In addition, it was shown in previous work [128] that the salt flux exacerbates the organic fouling. Consequently, minimizing the salt diffusion by using draw solutions that guarantee low reversal salt flux can be considered as a tool for fouling mitigation. Therefore, organic draw solutions seem to be more suitable to extract maximum energy production using closed-loop PRO. In addition, as the increase of the operating temperature enhances the PRO process, the use of heat waste or warm water sources such as geothermal water or the discharge from central heating and air conditioning can raise the solution temperature of full-scale PRO, which is an effective way to harvest more clean energy and reduce energy waste.

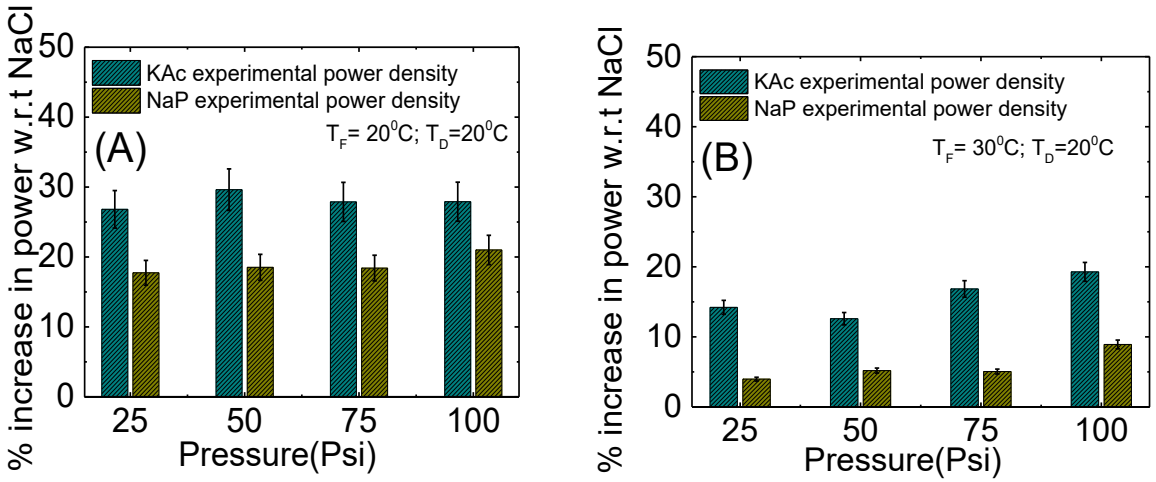

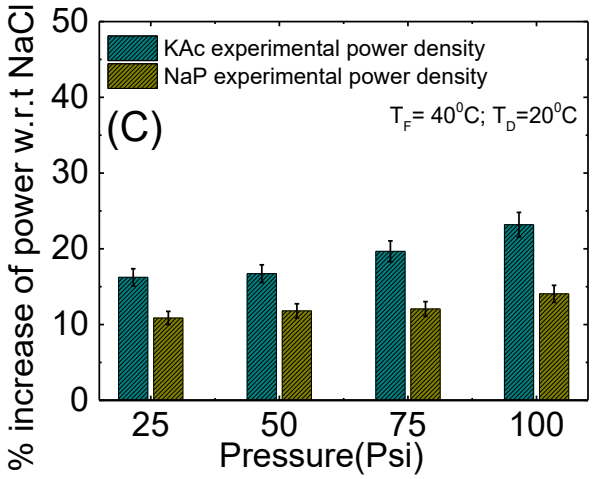

Figure 17 Percent increase of power density of draw solutions of KAc and NaP w.r.t NaCl as a function of draw solution pressure for different working temperatures A) T_F=20^{0}C, T_D=20^{0}C; B) T_F=30^{0}C, T_D=20^{0}C; C) T_F=40^{0}C, T_D=20^{0}C. Draw and feed flow velocity was 0.50 liter/min

Table 11 Osmotic pressure for 1 M solution at different operating temperatures

	Osmotic Pressure, π (MPa)		
T (℃)	NaCl	KAc	NaP
20	4.46	4.12	4.02
30	4.60	4.32	4.20
40	4.76	4.45	4.31

4.6 Conclusions

In this study, the effect of the operating temperature on the performance of closed-loop PRO with a commercial TFC FO membrane has been analyzed comprehensively for a commonly used inorganic (NaCl) draw salt as well as organic salts (potassium acetate and sodium propionate). The experimental data were verified with a numerical model. It has been found that an increase in temperature was accompanied by an improvement of PRO performance in terms of water flux and power density. Furthermore, the increase of salt diffusion with an increase of temperature was very prominent for NaCl. Organic draw solutions revealed very low salt flux compared with NaCl draw solutions. It was also shown that the use of organic salt can reduce the salt flux up to 84.5% compared to inorganic salt. This reduction of salt diffusion has mitigated the effect of

concentration polarization (CP). Overall, the performance of the PRO process greatly enhanced when using organic draw solutions. The increase of feed solution temperature from 20^0C to 40^0C when operating with organic salts can increase the power generation up to 23% when compared with the most commonly used NaCl draw solution. This study revealed that combining the use of waste heat (to increase the operating temperature) and organic salts (as draw solution) may give a step forward to maximize the extractable energy from a closed-loop PRO process.

Chapter 5: Conclusion and Recommendations

For successful operation of the closed-loop PRO process, selection of a suitable draw solution is a prerequisite. In this study, extensive database-driven screening method has been adapted to identify potential organic draw solutions for the sustainability of the closed-loop process. Based on solubility, osmotic pressure, toxicity and physical state at ambient condition, organic compounds potassium citrate, calcium acetate, potassium oxalate, potassium acetate, ammonium acetate, ammonium carbamate, ammonium formate, potassium formate, sodium glycolate, sodium propionate and calcium propionate were identified for the first time as highly effective draw solutions (except for NaP).

After identifying the above-mentioned organic draw solutions, comprehensive experimental analysis has been conducted to evaluate the performance of the PRO system to determine the efficacy of the system. All the draw solutions (except for KCit) showed 1.06% to 18.69% and 6.9% to 25.56% higher peak power densities compared to NaCl and NH_4HCO_3, respectively, at 2.8 MPa osmotic pressure. A 50% increase of osmotic pressure to organic draw solutes are associated with a 109-118% rise in peak power density. Reversal salt flux for organic draw solutions was found to be significantly lower compared to most commonly used inorganic draw solutions like NaCl and NH_4HCO_3.

In this study, the effect of temperature on water and salt fluxes with a commercial TFC FO membrane has also been analyzed comprehensively for commonly used inorganic (NaCl) draw salt as well as organic salts (potassium acetate and sodium propionate) for a comparative study. Utilizing low-grade waste heat (raising temperature from 20^0 to 40^0C) increases the overall performance of the process by 34%, 31% and 27% for NaCl, KAc and NaP, respectively. From this research, it has been shown that the increase of feed solution temperature from 20^0C to 40^0C can increase the overall power generation by up to 23% when compared with the most commonly used NaCl draw solution.

However, the increase in the temperature is accompanied by an increase in the salt diffusion which is very prominent for NaCl. Conversely, for organic draw solutions, salt diffusion has been found

very low (5~8 times lower than NaCl). The results show that organic salt can reduce the salt flux. This reduction of salt flux is greatly associated with the reduction of concentration polarization (CP) phenomenon in PRO process. Due to this reduction of CP with the increase in operating temperature, the performance of the PRO process greatly enhanced when using the organic draw solutions

The selected organic draw solutions were also tested for a potential recovery method in the downstream of the PRO process. The laboratory investigation revealed that the membrane distillation and thermal distillation (at ~50 °C) techniques are potential recovery methods for the selected draw solutions (excluding NH_4Ac and NH_4F). The high peak power density and potential recovery methods associated with very lower reversal salt flux could make the selected organic draw solutions commercially viable for applications to the closed-loop PRO process.

Integration of closed-loop PRO with a real waste heat source, for example, solar panels, power plants etc. would be interesting to observe the viability of this process. Also, the calculation of net energy balance to investigate the efficiency of closed-loop PRO process could be done in the future. A careful balance between operational and capital costs followed by a detailed life cycle assessment should be performed in future before implementing closed-loop PRO for power generation. Development of more robust membrane to withstand high operating pressure can boost the acceptance of PRO power generation to the next level. In order to achieve this goal, surface modification, increasing internal diameters of the PRO membrane, developing less porous support layers, and novel spacers could be done on the future. Another very important feature for future research is to find alternative less energy intensive downstream separation process. Further investigations on draw solutions for higher yield in terms of power generation could also be done in future research.

References

[1] A. Achilli and A. E. Childress, "Pressure retarded osmosis: From the vision of Sidney Loeb to the first prototype installation — Review," *Desalination*, vol. 261, no. 3, pp. 205–211, Oct. 2010.

[2] M. S. Islam, S. Sultana, S. Adhikary, and M. S. Rahaman, "Highly effective organic draw solutions for renewable power generation by closed-loop pressure retarded osmosis," *Energy Convers. Manag.*, vol. 171, pp. 1226–1236, Sep. 2018.

[3] M. Xie, W. E. Price, L. D. Nghiem, and M. Elimelech, "Effects of feed and draw solution temperature and transmembrane temperature difference on the rejection of trace organic contaminants by forward osmosis," *J. Membr. Sci.*, vol. 438, pp. 57–64, Jul. 2013.

[4] R. E. Pattle, "Production of Electric Power by mixing Fresh and Salt Water in the Hydroelectric Pile," *Nature*, vol. 174, no. 4431, p. 660, Oct. 1954.

[5] H. D. S. S. Karunarathne and S. Walpalage, "Applicability of Pressure Retarded Osmosis Power Generation Technology in Sri Lanka," *Energy Procedia*, vol. 34, pp. 211–217, Jan. 2013.

[6] Q. She, X. Jin, and C. Y. Tang, "Osmotic power production from salinity gradient resource by pressure retarded osmosis: Effects of operating conditions and reverse solute diffusion," *J. Membr. Sci.*, vol. 401–402, pp. 262–273, May 2012.

[7] B. Al-Anzi, A. Thomas, and J. Fernandes, "Lab scale assessment of power generation using pressure retarded osmosis from wastewater treatment plants in the state of Kuwait," *Desalination*, vol. 396, pp. 57–69, Oct. 2016.

[8] R. S. Norman, "Water salination: a source of energy," *Science*, vol. 186, no. 4161, pp. 350–352, Oct. 1974.

[9] S. Loeb, F. Van Hessen, and D. Shahaf, "Production of energy from concentrated brines by pressure-retarded osmosis: II. Experimental results and projected energy costs," *J. Membr. Sci.*, vol. 1, pp. 249–269, Jan. 1976.

[10] S. Loeb and G. D. Mehta, "A two-coefficient water transport equation for pressure-retarded osmosis," *J. Membr. Sci.*, vol. 4, pp. 351–362, Jan. 1978.

[11] G. D. Mehta and S. Loeb, "Internal polarization in the porous substructure of a semipermeable membrane under pressure-retarded osmosis," *J. Membr. Sci.*, vol. 4, pp. 261–265, Jan. 1978.

[12] G. D. Mehta and S. Loeb, "Performance of permasep B-9 and B-10 membranes in various osmotic regions and at high osmotic pressures," *J. Membr. Sci.*, vol. 4, pp. 335–349, Jan. 1978.

[13] S. Loeb, "Production of energy from concentrated brines by pressure-retarded osmosis: I. Preliminary technical and economic correlations," *J. Membr. Sci.*, vol. 1, pp. 49–63, Jan. 1976.

[14] S. Loeb and R. S. Norman, "Osmotic Power Plants," *Science*, vol. 189, no. 4203, pp. 654–655, Aug. 1975.

[15] K. L. Lee, R. W. Baker, and H. K. Lonsdale, "Membranes for power generation by pressure-retarded osmosis," *J. Membr. Sci.*, vol. 8, no. 2, pp. 141–171, Jan. 1981.

[16] H. H. G. Jellinek and H. Masuda, "Osmo-power. Theory and performance of an osmo-power pilot plant," *Ocean Eng.*, vol. 8, no. 2, pp. 103–128, Jan. 1981.

[17] G. D. Mehta, "Further results on the performance of present-day osmotic membranes in various osmotic regions," *J. Membr. Sci.*, vol. 10, no. 1, pp. 3–19, Mar. 1982.

[18] F. Vigo and C. Uliana, “Suitability of reverse osmosis membranes for energy recovery by submarine osmotic power plants,” *Desalination*, vol. 60, no. 1, pp. 45–57, Jan. 1986.
[19] S. Loeb, T. Honda, and M. Reali, “Comparative mechanical efficiency of several plant configurations using a pressure-retarded osmosis energy converter,” *J. Membr. Sci.*, vol. 51, no. 3, pp. 323–335, Aug. 1990.
[20] M. Reali, G. Dassie, and G. Jonsson, “Computation of salt concentration profiles in the porous substrate of anisotropic membranes under steady pressure-retarded-osmosis conditions,” *J. Membr. Sci. - J Membr. SCI*, vol. 48, pp. 181–201, Feb. 1990.
[21] S. Loeb, “Energy production at the Dead Sea by pressure-retarded osmosis: challenge or chimera?,” *Desalination*, vol. 120, no. 3, pp. 247–262, Dec. 1998.
[22] “U.S. Energy Information Administration (EIA) - Total Energy Annual Data.” [Online]. Available: https://www.eia.gov/totalenergy/data/annual/. [Accessed: 27-Sep-2018].
[23] S. Loeb, “One hundred and thirty benign and renewable megawatts from Great Salt Lake? The possibilities of hydroelectric power by pressure-retarded osmosis,” *Desalination*, vol. 141, no. 1, pp. 85–91, Dec. 2001.
[24] S. Loeb, “Large-scale power production by pressure-retarded osmosis, using river water and sea water passing through spiral modules,” *Desalination*, vol. 143, no. 2, pp. 115–122, May 2002.
[25] A. Seppälä and M. J. Lampinen, “On the non-linearity of osmotic flow,” *Exp. Therm. Fluid Sci.*, vol. 28, no. 4, pp. 283–296, Mar. 2004.
[26] B. E. Logan and M. Elimelech, “Membrane-based processes for sustainable power generation using water,” *Nature*, vol. 488, no. 7411, pp. 313–319, Aug. 2012.
[27] N. Y. Yip *et al.*, “Thin-Film Composite Pressure Retarded Osmosis Membranes for Sustainable Power Generation from Salinity Gradients,” *Environ. Sci. Technol.*, vol. 45, no. 10, pp. 4360–4369, May 2011.
[28] S. van der Zwan, I. W. M. Pothof, B. Blankert, and J. I. Bara, “Feasibility of osmotic power from a hydrodynamic analysis at module and plant scale,” *J. Membr. Sci.*, vol. 389, pp. 324–333, Feb. 2012.
[29] Q. She, D. Hou, J. Liu, K. H. Tan, and C. Y. Tang, “Effect of feed spacer induced membrane deformation on the performance of pressure retarded osmosis (PRO): Implications for PRO process operation,” *J. Membr. Sci.*, vol. 445, pp. 170–182, Oct. 2013.
[30] D. Xiao, C. Y. Tang, J. Zhang, W. C. L. Lay, R. Wang, and A. G. Fane, “Modeling salt accumulation in osmotic membrane bioreactors: Implications for FO membrane selection and system operation,” *J. Membr. Sci.*, vol. 366, no. 1, pp. 314–324, Jan. 2011.
[31] J. L. Prante, J. A. Ruskowitz, A. E. Childress, and A. Achilli, “RO-PRO desalination: An integrated low-energy approach to seawater desalination,” *Appl. Energy*, vol. 120, pp. 104–114, May 2014.
[32] S. Lin, N. Y. Yip, T. Y. Cath, C. O. Osuji, and M. Elimelech, “Hybrid pressure retarded osmosis-membrane distillation system for power generation from low-grade heat: thermodynamic analysis and energy efficiency,” *Environ. Sci. Technol.*, vol. 48, no. 9, pp. 5306–5313, May 2014.
[33] A. Altaee and N. Hilal, “Dual-stage forward osmosis/pressure retarded osmosis process for hypersaline solutions and fracking wastewater treatment,” *Desalination*, vol. 350, pp. 79–85, Oct. 2014.
[34] G. Han, S. Zhang, X. Li, and T.-S. Chung, “Progress in pressure retarded osmosis (PRO) membranes for osmotic power generation,” *Prog. Polym. Sci.*, vol. 51, pp. 1–27, Dec. 2015.

[35] A. Altaee, G. Zaragoza, and A. Sharif, “Pressure retarded osmosis for power generation and seawater desalination: Performance analysis,” *Desalination*, vol. 344, pp. 108–115, Jul. 2014.
[36] A. Achilli, T. Y. Cath, and A. E. Childress, “Power generation with pressure retarded osmosis: An experimental and theoretical investigation,” *J. Membr. Sci.*, vol. 343, no. 1, pp. 42–52, Nov. 2009.
[37] N.-N. Bui and J. R. McCutcheon, “Nanofiber Supported Thin-Film Composite Membrane for Pressure-Retarded Osmosis,” *Environ. Sci. Technol.*, vol. 48, no. 7, pp. 4129–4136, Apr. 2014.
[38] X. Wang, Z. Huang, L. Li, S. Huang, E. H. Yu, and K. Scott, “Energy Generation from Osmotic Pressure Difference Between the Low and High Salinity Water by Pressure Retarded Osmosis,” *J. Technol. Innov. Renew. Energy*, vol. 1, no. 2, pp. 122–130, Jan. 2013.
[39] J. R. McCutcheon and M. Elimelech, “Influence of membrane support layer hydrophobicity on water flux in osmotically driven membrane processes,” *J. Membr. Sci.*, vol. 318, no. 1, pp. 458–466, Jun. 2008.
[40] S. LOEB, “The Loeb-Sourirajan Membrane: How It Came About,” in *Synthetic Membranes:*, vol. 153, 0 vols., AMERICAN CHEMICAL SOCIETY, 1981, pp. 1–9.
[41] K. Touati and F. Tadeo, “Green energy generation by pressure retarded osmosis: State of the art and technical advancement—review,” *Int. J. Green Energy*, vol. 14, no. 4, pp. 337–360, Mar. 2017.
[42] X. Song, Z. Liu, and D. D. Sun, “Energy recovery from concentrated seawater brine by thin-film nanofiber composite pressure retarded osmosis membranes with high power density,” *Energy Environ. Sci.*, vol. 6, no. 4, pp. 1199–1210, Mar. 2013.
[43] D. T. Clausi and W. J. Koros, “Formation of defect-free polyimide hollow fiber membranes for gas separations,” *J. Membr. Sci.*, vol. 167, no. 1, pp. 79–89, Mar. 2000.
[44] S. Chou, R. Wang, L. Shi, Q. She, C. Tang, and A. G. Fane, “Thin-film composite hollow fiber membranes for pressure retarded osmosis (PRO) process with high power density,” *J. Membr. Sci.*, vol. 389, pp. 25–33, Feb. 2012.
[45] G. Han and T.-S. Chung, “Robust and high performance pressure retarded osmosis hollow fiber membranes for osmotic power generation,” *AIChE J.*, vol. 60, no. 3, pp. 1107–1119.
[46] X. Li and T.-S. Chung, “Thin-film composite P84 co-polyimide hollow fiber membranes for osmotic power generation,” *Appl. Energy*, vol. 114, pp. 600–610, Feb. 2014.
[47] P. G. Ingole *et al.*, “Preparation, characterization and performance evaluations of thin film composite hollow fiber membrane for energy generation,” *Desalination*, vol. 345, pp. 136–145, Jul. 2014.
[48] Q. Ge, M. Ling, and T.-S. Chung, “Draw solutions for forward osmosis processes: Developments, challenges, and prospects for the future,” *J. Membr. Sci.*, vol. 442, pp. 225–237, Sep. 2013.
[49] G. Han, Q. Ge, and T.-S. Chung, “Conceptual demonstration of novel closed-loop pressure retarded osmosis process for sustainable osmotic energy generation,” *Appl. Energy*, vol. 132, pp. 383–393, Nov. 2014.
[50] D. Attarde, M. Jain, K. Chaudhary, and S. K. Gupta, “Osmotically driven membrane processes by using a spiral wound module — Modeling, experimentation and numerical parameter estimation,” *Desalination*, vol. 361, pp. 81–94, Apr. 2015.
[51] Y. C. Kim and M. Elimelech, “Potential of osmotic power generation by pressure retarded osmosis using seawater as feed solution: Analysis and experiments,” *J. Membr. Sci.*, vol. 429, pp. 330–337, Feb. 2013.

[52] H. Gong, D. D. Anastasio, K. Wang, and J. R. McCutcheon, “Finding better draw solutes for osmotic heat engines: Understanding transport of ions during pressure retarded osmosis,” *Desalination*, vol. 421, pp. 32–39, Nov. 2017.
[53] K. L. Hickenbottom, J. Vanneste, and T. Y. Cath, “Assessment of alternative draw solutions for optimized performance of a closed-loop osmotic heat engine,” *J. Membr. Sci.*, vol. 504, pp. 162–175, Apr. 2016.
[54] E. Shaulsky, C. Boo, S. Lin, and M. Elimelech, “Membrane-based osmotic heat engine with organic solvent for enhanced power generation from low-grade heat,” *Environ. Sci. Technol.*, vol. 49, no. 9, pp. 5820–5827, May 2015.
[55] “Membrane distillation,” *Wikipedia*. 26-Jul-2018.
[56] “Waste Heat Recovery: Technology and Opportunities in U.S. Industry,” p. 112.
[57] M. Irandoust, “The renewable energy-growth nexus with carbon emissions and technological innovation: Evidence from the Nordic countries,” *Ecol. Indic.*, vol. 69, pp. 118–125, Oct. 2016.
[58] Y. Yang, H. S. Solgaard, and W. Haider, “Wind, hydro or mixed renewable energy source: Preference for electricity products when the share of renewable energy increases,” *Energy Policy*, vol. 97, pp. 521–531, Oct. 2016.
[59] M. A. Destek, “Renewable energy consumption and economic growth in newly industrialized countries: Evidence from asymmetric causality test,” *Renew. Energy*, vol. 95, pp. 478–484, Sep. 2016.
[60] I. A. Nienhueser and Y. Qiu, “Economic and environmental impacts of providing renewable energy for electric vehicle charging – A choice experiment study,” *Appl. Energy*, vol. 180, pp. 256–268, Oct. 2016.
[61] S. Bahramara, M. P. Moghaddam, and M. R. Haghifam, “Optimal planning of hybrid renewable energy systems using HOMER: A review,” *Renew. Sustain. Energy Rev.*, vol. 62, pp. 609–620, Sep. 2016.
[62] T. YuChing, C. YeaKuang, K. FuKuang, and Y. JingTang, “Integrated operation of renewable energy sources and water resources.,” *Energy Convers. Manag.*, vol. 160, pp. 439–454, 2018.
[63] A. García-Olivares, J. Solé, and O. Osychenko, “Transportation in a 100% renewable energy system,” *Energy Convers. Manag.*, vol. 158, pp. 266–285, Feb. 2018.
[64] G. Liu, M. Li, B. Zhou, Y. Chen, and S. Liao, “General indicator for techno-economic assessment of renewable energy resources,” *Energy Convers. Manag.*, vol. 156, pp. 416–426, Jan. 2018.
[65] M. Lv, J. Li, W. Zhu, H. Du, J. Meng, and K. Sun, “A theoretical study of rotatable renewable energy system for stratospheric airship,” *Energy Convers. Manag.*, vol. 140, pp. 51–61, May 2017.
[66] T.-S. Chung, L. Luo, C. F. Wan, Y. Cui, and G. Amy, “What is next for forward osmosis (FO) and pressure retarded osmosis (PRO),” *Sep. Purif. Technol.*, vol. 156, pp. 856–860, Dec. 2015.
[67] A. Achilli, J. L. Prante, N. T. Hancock, E. B. Maxwell, and A. E. Childress, “Experimental Results from RO-PRO: A Next Generation System for Low-Energy Desalination,” *Environ. Sci. Technol.*, vol. 48, no. 11, pp. 6437–6443, Jun. 2014.
[68] T. Thorsen and T. Holt, “The potential for power production from salinity gradients by pressure retarded osmosis,” *J. Membr. Sci.*, vol. 335, no. 1, pp. 103–110, Jun. 2009.

[69] T.-S. Chung, X. Li, R. C. Ong, Q. Ge, H. Wang, and G. Han, "Emerging forward osmosis (FO) technologies and challenges ahead for clean water and clean energy applications," *Curr. Opin. Chem. Eng.*, vol. 1, no. 3, pp. 246–257, Aug. 2012.
[70] S. E. Skilhagen, J. E. Dugstad, and R. J. Aaberg, "Osmotic power — power production based on the osmotic pressure difference between waters with varying salt gradients," *Desalination*, vol. 220, no. 1, pp. 476–482, Mar. 2008.
[71] S. E. Skilhagen, "Osmotic power — a new, renewable energy source," *Desalination Water Treat.*, vol. 15, no. 1–3, pp. 271–278, Mar. 2010.
[72] R. L. McGinnis, J. R. McCutcheon, and M. Elimelech, "A novel ammonia–carbon dioxide osmotic heat engine for power generation," *J. Membr. Sci.*, vol. 305, no. 1, pp. 13–19, Nov. 2007.
[73] G. Han, J. Zuo, C. Wan, and T.-S. Chung, "Hybrid pressure retarded osmosis–membrane distillation (PRO–MD) process for osmotic power and clean water generation," *Environ. Sci. Water Res. Technol.*, vol. 1, no. 4, pp. 507–515, Jul. 2015.
[74] G. Han, Q. Ge, and T.-S. Chung, "Conceptual demonstration of novel closed-loop pressure retarded osmosis process for sustainable osmotic energy generation," *Appl. Energy*, vol. 132, pp. 383–393, Nov. 2014.
[75] Q. Ge, M. Ling, and T.-S. Chung, "Draw solutions for forward osmosis processes: Developments, challenges, and prospects for the future," *J. Membr. Sci.*, vol. 442, pp. 225–237, Sep. 2013.
[76] A. Achilli, T. Y. Cath, and A. E. Childress, "Selection of inorganic-based draw solutions for forward osmosis applications," *J. Membr. Sci.*, vol. 364, no. 1, pp. 233–241, Nov. 2010.
[77] M. L. Stone, A. D. Wilson, M. K. Harrup, and F. F. Stewart, "An initial study of hexavalent phosphazene salts as draw solutes in forward osmosis," *Desalination*, vol. 312, pp. 130–136, Mar. 2013.
[78] S. K. Yen, F. Mehnas Haja N., M. Su, K. Y. Wang, and T.-S. Chung, "Study of draw solutes using 2-methylimidazole-based compounds in forward osmosis," *J. Membr. Sci.*, vol. 364, no. 1, pp. 242–252, Nov. 2010.
[79] K. S. Bowden, A. Achilli, and A. E. Childress, "Organic ionic salt draw solutions for osmotic membrane bioreactors," *Bioresour. Technol.*, vol. 122, pp. 207–216, Oct. 2012.
[80] B. Corzo, T. de la Torre, C. Sans, E. Ferrero, and J. J. Malfeito, "Evaluation of draw solutions and commercially available forward osmosis membrane modules for wastewater reclamation at pilot scale," *Chem. Eng. J.*, vol. 326, pp. 1–8, Oct. 2017.
[81] G. Han, Z. L. Cheng, and T.-S. Chung, "Thin-film composite (TFC) hollow fiber membrane with double-polyamide active layers for internal concentration polarization and fouling mitigation in osmotic processes," *J. Membr. Sci.*, vol. 523, pp. 497–504, Feb. 2017.
[82] D. Emadzadeh, W. J. Lau, T. Matsuura, M. Rahbari-Sisakht, and A. F. Ismail, "A novel thin film composite forward osmosis membrane prepared from PSf–TiO2 nanocomposite substrate for water desalination," *Chem. Eng. J.*, vol. 237, pp. 70–80, Feb. 2014.
[83] L. Shen, S. Xiong, and Y. Wang, "Graphene oxide incorporated thin-film composite membranes for forward osmosis applications," *Chem. Eng. Sci.*, vol. 143, pp. 194–205, Apr. 2016.
[84] S. Loeb, L. Titelman, E. Korngold, and J. Freiman, "Effect of porous support fabric on osmosis through a Loeb-Sourirajan type asymmetric membrane," *J. Membr. Sci.*, vol. 129, no. 2, pp. 243–249, Jul. 1997.

[85] Y. C. Kim, Y. Kim, D. Oh, and K. H. Lee, "Experimental Investigation of a Spiral-Wound Pressure-Retarded Osmosis Membrane Module for Osmotic Power Generation," *Environ. Sci. Technol.*, vol. 47, no. 6, pp. 2966–2973, Mar. 2013.
[86] S.-F. Pan, Y. Dong, Y.-M. Zheng, L.-B. Zhong, and Z.-H. Yuan, "Self-sustained hydrophilic nanofiber thin film composite forward osmosis membranes: Preparation, characterization and application for simulated antibiotic wastewater treatment," *J. Membr. Sci.*, vol. 523, pp. 205–215, Feb. 2017.
[87] C. Boo, Y. F. Khalil, and M. Elimelech, "Performance evaluation of trimethylamine–carbon dioxide thermolytic draw solution for engineered osmosis," *J. Membr. Sci.*, vol. 473, pp. 302–309, Jan. 2015.
[88] C. F. Wan and T.-S. Chung, "Energy recovery by pressure retarded osmosis (PRO) in SWRO–PRO integrated processes," *Appl. Energy*, vol. 162, pp. 687–698, Jan. 2016.
[89] A. P. Straub, N. Y. Yip, and M. Elimelech, "Raising the Bar: Increased Hydraulic Pressure Allows Unprecedented High Power Densities in Pressure-Retarded Osmosis," *Environ. Sci. Technol. Lett.*, vol. 1, no. 1, pp. 55–59, Jan. 2014.
[90] K. L. Hickenbottom, J. Vanneste, M. Elimelech, and T. Y. Cath, "Assessing the current state of commercially available membranes and spacers for energy production with pressure retarded osmosis," *Desalination*, vol. 389, pp. 108–118, Jul. 2016.
[91] "ACETAMIDE," *Org. Synth.*, vol. 3, p. 3, 1923.
[92] *The Chemical News and Journal of Industrial Science*. 1864.
[93] R. D. Shannon, "Revised effective ionic radii and systematic studies of interatomic distances in halides and chalcogenides," *Acta Crystallogr. A*, vol. 32, no. 5, pp. 751–767, Sep. 1976.
[94] D. L. Shaffer, L. H. Arias Chavez, M. Ben-Sasson, S. Romero-Vargas Castrillón, N. Y. Yip, and M. Elimelech, "Desalination and Reuse of High-Salinity Shale Gas Produced Water: Drivers, Technologies, and Future Directions," *Environ. Sci. Technol.*, vol. 47, no. 17, pp. 9569–9583, Sep. 2013.
[95] Y. Kim, J. H. Lee, Y. C. Kim, K. H. Lee, I. S. Park, and S.-J. Park, "Operation and simulation of pilot-scale forward osmosis desalination with ammonium bicarbonate," *Chem. Eng. Res. Des.*, vol. 94, pp. 390–395, Feb. 2015.
[96] L. F. Audrieta, H. Bluestone, L. A. Brooks, and W. C. Jofinsox, "Ammonium Carbamate," *Inorg Synth*, vol. 2, p. 85, 2007.
[97] B. Mi and M. Elimelech, "Chemical and physical aspects of organic fouling of forward osmosis membranes," *J. Membr. Sci.*, vol. 320, no. 1, pp. 292–302, Jul. 2008.
[98] S. Lee and Y. C. Kim, "Calcium carbonate scaling by reverse draw solute diffusion in a forward osmosis membrane for shale gas wastewater treatment," *J. Membr. Sci.*, vol. 522, pp. 257–266, Jan. 2017.
[99] M. Bystrianský *et al.*, "The presence of ferric iron promotes calcium sulphate scaling in reverse osmosis processes," *Desalination*, vol. 393, pp. 115–119, Sep. 2016.
[100] S. L. Dixon, *Fluid mechanics and thermodynamics of turbomachinery*, 4th ed. in SI/metric units. Boston: Butterworth-Heinemann, 1998.
[101] A. H. Elbatran, O. B. Yaakob, Y. M. Ahmed, and H. M. Shabara, "Operation, performance and economic analysis of low head micro-hydropower turbines for rural and remote areas: A review," *Renew. Sustain. Energy Rev.*, vol. 43, pp. 40–50, Mar. 2015.
[102] "GECO2017.pdf." .

[103] B. Ekwurzel *et al.*, "The rise in global atmospheric CO2, surface temperature, and sea level from emissions traced to major carbon producers," *Clim. Change*, vol. 144, no. 4, pp. 579–590, Oct. 2017.
[104] "Turning to renewables: Climate-safe energy solutions," */publications/2017/Nov/Turning-to-renewables-Climate-safe-energy-solutions*. [Online]. Available: /publications/2017/Nov/Turning-to-renewables-Climate-safe-energy-solutions. [Accessed: 27-Sep-2018].
[105] J. Kim, J. Lee, and J. H. Kim, "Overview of pressure-retarded osmosis (PRO) process and hybrid application to sea water reverse osmosis process," *Desalination Water Treat.*, vol. 43, no. 1–3, pp. 193–200, Apr. 2012.
[106] X. Liu, L.-X. Foo, Y. Li, J.-Y. Lee, B. Cao, and C. Y. Tang, "Fabrication and characterization of nanocomposite pressure retarded osmosis (PRO) membranes with excellent anti-biofouling property and enhanced water permeability," *Desalination*, vol. 389, pp. 137–148, Jul. 2016.
[107] Q. She *et al.*, "Fabrication and characterization of fabric-reinforced pressure retarded osmosis membranes for osmotic power harvesting," *J. Membr. Sci.*, vol. 504, pp. 75–88, Apr. 2016.
[108] M. Tian, R. Wang, K. Goh, Y. Liao, and A. G. Fane, "Synthesis and characterization of high-performance novel thin film nanocomposite PRO membranes with tiered nanofiber support reinforced by functionalized carbon nanotubes," *J. Membr. Sci.*, vol. 486, pp. 151–160, Jul. 2015.
[109] G. Han, P. Wang, and T.-S. Chung, "Highly Robust Thin-Film Composite Pressure Retarded Osmosis (PRO) Hollow Fiber Membranes with High Power Densities for Renewable Salinity-Gradient Energy Generation," *Environ. Sci. Technol.*, vol. 47, no. 14, pp. 8070–8077, Jul. 2013.
[110] A. Altaee, P. Palenzuela, G. Zaragoza, and A. A. AlAnezi, "Single and dual stage closed-loop pressure retarded osmosis for power generation: Feasibility and performance," *Appl. Energy*, vol. 191, pp. 328–345, Apr. 2017.
[111] K. Touati, F. Tadeo, and H. Elfil, "Osmotic energy recovery from Reverse Osmosis using two-stage Pressure Retarded Osmosis," *Energy*, vol. 132, pp. 213–224, Aug. 2017.
[112] C. F. Wan and T.-S. Chung, "Maximize the operating profit of a SWRO-PRO integrated process for optimal water production and energy recovery," *Renew. Energy*, vol. 94, pp. 304–313, Aug. 2016.
[113] K. Touati, J. Salamanca, F. Tadeo, and H. Elfil, "Energy recovery from two-stage SWRO plant using PRO without external freshwater feed stream: Theoretical analysis," *Renew. Energy*, vol. 105, pp. 84–95, May 2017.
[114] W. He, Y. Wang, V. Elyasigomari, and M. H. Shaheed, "Evaluation of the detrimental effects in osmotic power assisted reverse osmosis (RO) desalination," *Renew. Energy*, vol. 93, pp. 608–619, Aug. 2016.
[115] K. Touati and F. Tadeo, "Study of the Reverse Salt Diffusion in pressure retarded osmosis: Influence on concentration polarization and effect of the operating conditions," *Desalination*, vol. 389, pp. 171–186, Jul. 2016.
[116] J. Maisonneuve, P. Pillay, and C. B. Laflamme, "Pressure-retarded osmotic power system model considering non-ideal effects," *Renew. Energy*, vol. 75, pp. 416–424, Mar. 2015.
[117] M. Li, "Optimization of multi-stage hybrid RO-PRO membrane processes at the water–energy nexus," *Chem. Eng. Res. Des.*, vol. 137, pp. 1–9, Sep. 2018.

[118] K. Touati, F. Tadeo, C. Hänel, and T. Schiestel, "Effect of the operating temperature on hydrodynamics and membrane parameters in pressure retarded osmosis," *Desalination Water Treat.*, vol. 57, no. 23, pp. 10477–10489, May 2016.
[119] K. Touati, C. Hänel, F. Tadeo, and T. Schiestel, "Effect of the feed and draw solution temperatures on PRO performance: Theoretical and experimental study," *Desalination*, vol. 365, pp. 182–195, Jun. 2015.
[120] D. D. Anastasio, J. T. Arena, E. A. Cole, and J. R. McCutcheon, "Impact of temperature on power density in closed-loop pressure retarded osmosis for grid storage," *J. Membr. Sci.*, vol. 479, pp. 240–245, Apr. 2015.
[121] E. Sivertsen, T. Holt, and W. R. Thelin, "Concentration and Temperature Effects on Water and Salt Permeabilities in Osmosis and Implications in Pressure-Retarded Osmosis," *Membranes*, vol. 8, no. 3, Jul. 2018.
[122] M. R. Chowdhury and J. R. McCutcheon, "Elucidating the impact of temperature gradients across membranes during forward osmosis: Coupling heat and mass transfer models for better prediction of real osmotic systems," *J. Membr. Sci.*, vol. 553, pp. 189–199, May 2018.
[123] J. R. McCutcheon and M. Elimelech, "Influence of concentrative and dilutive internal concentration polarization on flux behavior in forward osmosis," *J. Membr. Sci.*, vol. 284, no. 1, pp. 237–247, Nov. 2006.
[124] A. P. Straub, A. Deshmukh, and M. Elimelech, "Pressure-retarded osmosis for power generation from salinity gradients: is it viable?," *Energy Environ. Sci.*, vol. 9, no. 1, pp. 31–48, Jan. 2016.
[125] S. S. Manickam and J. R. McCutcheon, "Understanding mass transfer through asymmetric membranes during forward osmosis: A historical perspective and critical review on measuring structural parameter with semi-empirical models and characterization approaches," *Desalination*, vol. 421, pp. 110–126, Nov. 2017.
[126] A. P. Straub, C. O. Osuji, T. Y. Cath, and M. Elimelech, "Selectivity and Mass Transfer Limitations in Pressure-Retarded Osmosis at High Concentrations and Increased Operating Pressures," *Environ. Sci. Technol.*, vol. 49, no. 20, pp. 12551–12559, Oct. 2015.
[127] S. Lin, A. P. Straub, and M. Elimelech, "Thermodynamic limits of extractable energy by pressure retarded osmosis," *Energy Environ. Sci.*, vol. 7, no. 8, pp. 2706–2714, Jul. 2014.
[128] Q. She, Y. K. W. Wong, S. Zhao, and C. Y. Tang, "Organic fouling in pressure retarded osmosis: Experiments, mechanisms and implications," *J. Membr. Sci.*, vol. 428, pp. 181–189, Feb. 2013.